

An LTE effective temperature scale for red supergiants in the Magellanic clouds

H. M. Tabernero,^{1*} R. Dorda,¹ I. Negueruela¹ and C. González-Fernández^{1,2}

¹*Departamento de Física, Ingeniería de Sistemas y Teoría de la Señal, Universidad de Alicante, Carretera de San Vicente del Raspeig, E03690 Alicante, Spain*

²*Institute of Astronomy, University of Cambridge, Madingley Road, Cambridge CB3 0HA, United Kingdom*

Accepted XXX. Received YYY; in original form ZZZ

ABSTRACT

We present a self-consistent study of cool supergiants (CSGs) belonging to the Magellanic clouds. We calculated stellar atmospheric parameters using LTE KURUCZ and MARCS atmospheric models for more than 400 individual targets by fitting a careful selection of weak metallic lines. We explore the existence of a T_{eff} scale and its implications in two different metallicity environments (each Magellanic cloud). Critical and in-depth tests have been performed to assess the reliability of our stellar parameters (i.e. internal error budget, NLTE systematics). In addition, several Montecarlo tests have been carried out to infer the significance of the T_{eff} scale found. Our findings point towards a unique T_{eff} scale that seems to be independent of the environment.

Key words: stars: massive – stars: late-type – supergiants – Magellanic Clouds – stars: fundamental parameters

1 INTRODUCTION

Red supergiants (RSGs) are moderately high-mass stars (between ~ 10 and $40 M_{\odot}$) that have evolved to the cool side of the Hertzsprung-Russell diagram. The RSG phase represents the last (or at least one of the latest) step in their evolution. It covers only a small fraction of their lifespan, being a powerful constraint to test evolutionary tracks (see [Ekström et al. 2013](#)). Moreover, RSGs are the main progenitors of core-collapse supernovae (mostly Type IIp, but probably also other subtypes). For these reasons, the physical characterisation of these stars is fundamental in the understanding of their evolution. In this work we focus on the effective temperature (T_{eff}) of RSGs, which is an open question topic still today.

The temperature scale is the relation between the spectral type (SpT), which is a morphological classification, and T_{eff} . Classically, SpT classification of RSGs has been considered mostly related to the T_{eff} , as in other types of stars. However, a new interpretation of SpT has recently been proposed by [Davies et al. \(2013\)](#), and in this work, we revisit the T_{eff} scale to test the new scenario with a statistically significant sample of RSGs. This scale is important even today, because it is easier to obtain a SpT classification than a temperature in many cases: SpT can be derived from mid to low resolution spectra and it does not require a S/N as high as a

T_{eff} calculation. Moreover, not all groups have access to the resources necessary to derive precise temperatures. Although the SpT cannot supersede an T_{eff} calculation, knowing the relation between SpT and T_{eff} can be useful for many groups for the interpretation of their observations, especially in the case of large samples of RSGs.

Observational studies done in the last decades of the 20th century (e.g. [Lee 1970](#); [Humphreys & McElroy 1984](#)) presented relatively cool T_{eff} scales for RSGs, spanning from 4 300 K at K0 to 2 800 K at M5. Two decades later, [Massey & Olsen \(2003\)](#) derived a slightly different scale (with lower temperatures for K subtypes and higher ones for M subtypes). However, as they discussed, the T_{eff} scale they obtained is too cool when compared to contemporary evolutionary tracks ([Meynet & Maeder 2000](#)). A few years later, [Levesque et al. \(2005\)](#) revisited this topic. They employed synthetic spectra, generated using MARCS atmospheric models, against spectrophotometric observations of RSGs from the Milky Way (MW), covering the range from 4 000 to 9 500 Å. Their T_{eff} scale for MW RSGs, based on the overall shape of the flux-calibrated spectra and the depth of TiO bands, resulted in a better agreement with [Meynet & Maeder \(2000\)](#), since they derived warmer temperatures. Their temperature scale was also flatter than those in previous works, spanning from 4 100 K at K1 to 3 450 K at M5.

[Levesque et al. \(2006\)](#) also studied the RSGs from both the Large Magellanic Cloud (LMC) and the Small Magellanic Cloud (SMC). They used the same method as for the

* E-mail: htabernero@ua.es

MW (Levesque et al. 2005) to obtain a T_{eff} scale for each Magellanic Cloud (MC). Although their T_{eff} 's were closer to those present in evolutionary tracks than those of previous works on these galaxies (Massey & Olsen 2003), they still presented some disagreement, especially for the SMC. RSGs in both galaxies span a similar T_{eff} range: they range from ~ 4200 K at K1 to 3475 K at M2 for the SMC, while for the LMC the range was from ~ 4300 K at K1 to 3450 K at M4. Despite their similar values, typical temperatures of RSGs in each galaxy are substantially different, because each population has a different typical SpT. Humphreys (1979) had already found that the average SpT of a given population of RSGs has some dependence on its average metallicity, with later spectral types being found in higher metallicity environments. This effect has been widely confirmed within different galaxies (Elias et al. 1985; Massey & Olsen 2003; Levesque & Massey 2012; Dorda et al. 2016a), and also along the galactic plane of a given galaxy (M33; Drout et al. 2012). In consequence, the results of Levesque et al. (2006) indicate that RSGs from the SMC have a typical T_{eff} of ~ 3920 K, while it is ~ 3705 K in the case of the LMC.

Against these results, recently Davies et al. (2013) discussed the limitations of the methodology used by Levesque et al. (2005, 2006). They analysed a small spectrophotometric sample of stars from both MCs, obtaining their T_{eff} 's by using different methods. Firstly, they employed the same procedure as Levesque et al. (2006), by performing a global fit of their spectra to synthetic spectra generated using MARCS stellar atmospheric models. Since TiO bands dominate the appearance of RSG spectra in the optical region, they presented this method as a TiO scale. They also derived T_{eff} 's by fitting the optical and infrared (IR) spectral energy distribution (SED). Finally, they used the flux integration method (FIM) as a constraint for the two other methods. They found that the T_{eff} 's obtained by fitting MARCS-based synthetic spectra are significantly cooler than those obtained through the SED. They argued that the SED T_{eff} 's seem rather more reliable because of three strong arguments: i) MARCS T_{eff} 's were significantly cooler than those obtained through the FIM at the lowest interstellar reddening; ii) although the T_{eff} 's obtained through MARCS synthetic fitting reproduce well the TiO bands in the optical range, they overpredict the IR flux; and iii) they found no correlation between the reddening obtained through the TiO method and the diffuse interstellar bands measured. Moreover, their SED T_{eff} 's agree with Geneva evolutionary tracks. They argued that the discrepancies found between TiO T_{eff} 's and those from the other two methods are due to the behaviour of the TiO bands. The SpT sequence of late-types stars is classically defined by these bands. Thus, their strength had always been interpreted as a measurement of T_{eff} . Davies et al. (2013) concluded that an analysis based on TiO bands does not allow a correct derivation of T_{eff} , because these bands do not only respond to temperature, but are also affected by 3D effects and luminosity. The T_{eff} 's derived by Davies et al. (2013) through their preferred SED method span a surprisingly narrow range (4150 ± 150 K), regardless of the parental galaxy. From this, they suggested that the typical T_{eff} of RSGs of any given population does not depend on the metal content. They also suggested, contrary to the classical interpretation, that the SpT of RSGs is only depen-

dent on their evolutionary state. Thus, they imply that all RSGs have roughly the same T_{eff} , regardless of their SpT.

Since Davies et al. (2013) published their results, many other works have studied small samples of RSGs in different environments following the method originally proposed by Davies et al. (2010): atmospheric parameters are derived from the fit of a few atomic features in the *J*-band, where RSGs do not present strong molecular absorptions. This method has the advantage that it only uses photospheric features instead of molecular bands that are produced higher in the atmosphere. Therefore, their results are not affected by strong molecular absorptions. All these works found similar T_{eff} ranges for their samples, regardless of the typical metallicity of the parental environment: from 3800 K to 4100 K for the sample from Perseus OB1, in the Milky Way (Gazak et al. 2014); from 3790 K to 4000 K for NGC 6882 (Patrick et al. 2015); from 3760 K to 4030 K for NGC 2100, in the LMC (Patrick et al. 2016); and from 3800 K to 4200 K in the re-analysis of the Magellanic sample presented in Davies et al. (2013) with this method, which does not find any difference between the samples from the two galaxies (Davies et al. 2015). Finally, Gazak et al. (2015) studied RSGs from the spiral galaxy NGC 300 at multiple radial distances, and did not find any trend between metallicity (which covers 0.6 dex) and typical T_{eff} . All these works agree with the conclusion of Davies et al. (2013), because of the similarity of the T_{eff} ranges found.

Last year, we presented our analysis of two very large samples of cool supergiants (CSGs), one from the LMC and the other from the SMC (Dorda et al. 2016a). In total, our sample had more than 500 CSGs, including classical RSGs (with K and M types) but also G supergiants, which we concluded are a significant part of the same population of evolved high-mass stars as RSGs in the SMC. Our main objective was to test the hypothesis of Davies et al. (2013) about the lack of dependence between SpT and T_{eff} , and the relation of SpT with stellar luminosity and evolutionary stage (usually related to mass loss). For that work, we applied the recommendations of Davies et al. (2013) about the necessity of using atomic features from the photosphere for the spectral analysis instead of TiO bands. Therefore we used a long list of well-known atomic lines in the range of the infrared Calcium Triplet (CaT), from 8400\AA to 8900\AA . However, we did not derive stellar parameters directly from these lines. Instead, we studied their global behaviour, by comparing it with the theoretical dependence of line strengths on T_{eff} , luminosity, and metallicity. Our results provide indirect proof, although with high statistical significance, that there is a T_{eff} scale in CSGs; in other words, that SpT depends mainly on T_{eff} . However, we also found a secondary but clear dependence on luminosity (bolometric magnitude), which confirms for a significantly large sample a long suspected effect: more luminous CSGs typically tend to present later SpTs.

In this work we go a step further than previous works. We calculate T_{eff} and $[M/H]$ for most of the RSGs in the sample of Dorda et al. (2016a), which is much larger than any other sample previously used for this purpose. For this, we performed a careful empirical selection of atomic features. Our main objective is to prove if a connection between T_{eff} and SpTs exists. We take advantage of the statistically significant size of our sample. In addition, we want to study

the relation between the different stellar parameters in the CSG populations of both MCs. Finally, we will compare our results with theoretical evolutionary tracks of massive stars.

The sample that we employ in the present work is described in Sect. 2. Detailed explanations of the derivation of stellar parameters are given in Sect. 3. In Sect. 4 we discuss our results and compare them to those obtained in previous works, as well as to evolutionary tracks. Finally in Sect. 5, we summarize our conclusions about the existence of an T_{eff} scale for the CSGs studied in the present manuscript.

2 THE SAMPLE

The sample of CSGs analysed in this work has already been published in González-Fernández et al. (2015, Paper I), Dorda et al. (2016a, Paper II) and Dorda et al. (2016b, Paper III). In Paper I we presented and discussed the selection of targets, the observations and our classification using optical spectra. In Paper II, we analysed the sample of CSGs. We studied the empirical behaviour of atomic features present in the infrared Calcium Triplet (CaT) spectral region against SpT, luminosity, and mass loss. We also discussed the spectral variability of stars in our sample, their SpT distributions, and the implications of our results for the current understanding of CSGs. In Paper III, we employed these spectral features mentioned above to implement an automated method to identify CSGs through their spectra.

The observations are explained in detail in Paper I. Thus, here we will only summarize them. We used the fibered dual-beam AAOmega spectrograph on the 3.9 m Anglo-Australian Telescope on four separate runs between 2010 and 2103. Thanks to the dual-beam, all the targets were observed simultaneously in the optical and the CaT spectral ranges. The grating used for the infrared range was 1700D, which provides a 500 Å wide range, centred on 8600 Å in 2010 and on 8700 Å for all other epochs. This grating has a nominal resolving power ($\lambda/\delta\lambda$) of 10000 at the wavelengths considered. The gratings for the optical range have no bearing on the present work; their details are provided in table 1 of Paper I.

Spectra in the optical range were used to infer the SpT and luminosity class (LC) for all the targets observed (see Paper I, for details). We used classical criteria based on atomic line ratios and TiO band depths, when present in the spectra. We also used radial velocities (RV) alongside our LC classification to confirm their membership to the MCs (see figs. 5 and 6 from Paper I). Some targets were observed at least twice within the same epoch. If so, final SpT and LC classifications for each target at each epoch were calculated using a S/N-weighted average.

Since the optical range is crowded with molecular features (mainly from TiO), the characterization of the spectra of these stars becomes difficult, due to effects like the lack of a visible continuum. We decided to tackle the problem in two fronts. Firstly, we restricted the spectral range to the CaT spectral region that is much less affected by TiO bands than the blue or red regions and contains a large number of well-resolved weak atomic lines. Secondly, we imposed a cut based on our previously derived SpTs. In the CaT range, molecular bands are not noticeable for types earlier than M1. Moreover, atomic lines become significantly eroded by

these absorption bands on the continuum only for types later than M3 (see sect. 2.2 and fig. 1 in Paper I). Therefore, here we only use stars with SpT M3 or earlier. This limitation excludes only 8.3% of the CSGs (most of them from the LMC). The statistical significance of the sample is not compromised. While most previous works on this topic centre their efforts on K and M supergiants, denominated as RSGs (See Sect. 1), we also include the G supergiants in the sample analysed in this paper, since in Paper II we demonstrated that these yellow supergiants (YSGs) are part of the same population as RSGs in the SMC. Thus, we refer to the stars in our sample as CSGs, which includes G, K and M types. In addition, we truncated the sample by leaving out every spectrum with an average S/N lower than 30, in order to obtain a minimum quality for our derived stellar atmospheric parameters. In Section 3.3 we discuss further the effect of low S/N on the parameter uncertainties.

The bolometric magnitudes of our targets were calculated through the bolometric correction of Bessell & Wood (1984), which is derived from the ($J - K$) color index. We used the 2MASS photometry (Skrutskie et al. 2006) for this calculation, previously transforming it to the AAO system used by Bessell & Wood (1984). We have assumed that the effect of the reddening on this calibration is negligible (see section 2.2 of Paper II, for more details). The absolute bolometric magnitudes were calculated using the following distance modulus to the MCs: $\mu = 18.48 \pm 0.05$ mag for the LMC (Walker 2012) and $\mu = 18.99 \pm 0.07$ mag for the SMC (Graczyk et al. 2014).

3 SPECTROSCOPIC ANALYSIS

All spectra were normalized using the CONTINUUM task within IRAF¹. Later, we shifted the spectra into the rest-frame using the radial velocities already calculated in Paper I, through the IRAF DOPCOR task.

3.1 Stellar Parameters

Stellar atmospheric parameters and abundances were computed using a previously generated grid of synthetic spectra (see Sect. 3.2 and Table A2). We employed a modified version of the automated code STEPAR (see Taberner et al. 2012). The new version relies upon spectral synthesis instead of equivalent widths (EWs). We also replaced the original optimization method (based on a downhill simplex algorithm) with a Metropolis-Hastings algorithm using Markov chains (Metropolis et al. 1953). Our method generates a Markov-Chain of 20000 points starting from an arbitrary point. To be able to evaluate any point within the stellar parameter space, we employed a bilinear interpolation scheme. As objective function we used a χ -squared in order to fit any previously selected spectral features.

The present version of STEPAR allows the simultaneous derivation of any set of stellar atmospheric parameters.

¹ IRAF is distributed by the National Optical Astronomy Observatories, which are operated by the Association of Universities for Research in Astronomy, Inc., under cooperative agreement with the National Science Foundation.

In this case we restricted them to only two variables, T_{eff} and metallicity ($[M/H]$). Surface gravity ($\log g$) was kept fixed to 0.0 dex, microturbulence (ξ) was also kept constant at 3 km s^{-1} , according to the approximation discussed by [García-Hernández et al. \(2007\)](#). Our analysis revolves around a few atomic features in the spectral range around the CaT, from 8400 to 8900 Å. We employed some empirically selected lines of Mg, Si, Ti, and Fe (see Section 3.2). We also convolved our grid of synthetic spectra with a gaussian kernel ($\text{FWHM} \approx 30 \text{ km s}^{-1}$) to account for the instrumental broadening.

3.2 Synthetic spectra

The synthetic spectra were generated using two sets of one-dimensional LTE atmospheric models, namely: ATLAS-APOGEE (KURUCZ) plane-parallel models ([Mészáros et al. 2012](#)), and MARCS spherical models with $15 M_{\odot}$ ([Gustafsson et al. 2008](#)). The radiative transfer code employed was *spectrum* ([Gray & Corbally 1994](#)). Also, we employed the abundances of [Asplund et al. \(2005\)](#) as Solar reference (namely, $Z_{\odot} = 0.0122$). Although MARCS atmospheric models are spherical, *spectrum* treats them as if they were plane-parallel. This can lead to a small inconsistency in the synthetic spectrum calculations. However, the study by [Heiter & Eriksson \(2006\)](#) concluded that any difference introduced by the spherical models in a plane-parallel transport scheme is not significant. As line list, we employed a selection from the VALD database ([Piskunov et al. 1995](#); [Kupka et al. 2000](#); [Ryabchikova et al. 2015](#)), taking into account all the relevant atomic and molecular features (dominated by TiO and CN) that can appear in CSGs with SpT M3 or earlier. Atomic data for the most prominent atomic features and synthesis ranges employed can be found in Table A1. In addition, as Van der Waals damping prescription we employed the Anstee, Barklem, and O'Mara theory (ABO), when available in VALD (see [Barklem et al. 2000](#)). The grid of synthetic spectra was generated for a single $\log g = 0$ dex. Effective temperature T_{eff} ranges from 3500 K to 6000 K with a step of 250 K for the spectra generated using KURUCZ atmospheric models, whereas, for MARCS synthetic models, T_{eff} varies from 3300 K to 4500 K; the step is 250 K above 4000 K and 100 K otherwise. The microturbulence (ξ) was fixed to 3 km s^{-1} , see Sect. 3.1. Finally, the metallicity ranges from $[M/H] = -1.5$ dex to $[M/H] = 1.0$ dex in 0.25 dex steps for KURUCZ models, whereas MARCS models cover only from $[M/H] = -1.0$ dex to $[M/H] = 0.5$ dex, in 0.25 dex increments.

3.3 Final results and error budget

Uncertainties on the stellar parameters are derived from the statistics of the Markov Chain. Firstly, we chose only the second half of the chain. Secondly, we divided the chain into sequences of five points, and we took only the first point of each sequence. Then we generated histograms with those points using either T_{eff} or $[M/H]$. Errors and mean values were obtained by fitting a gaussian to each histogram. Points were combined into intervals according to the rule described in [Freedman & Diaconis \(1981\)](#). Typical errors are shown in Table 1. In addition, we show our best-fits synthetic models for seven high S/N spectra in Fig. A1. In general terms, our

Table 1. Typical uncertainties of the sample.

S/N	< 50	≥ 50	≥ 100	All
ΔT_{eff} (K)	493	169	114	172
$\Delta[M/H]$ (dex)	0.47	0.16	0.11	0.17
Spectra	10	905	629	915

internal uncertainties are dominated by two main sources. The first contribution comes from the assumptions intrinsic to any stellar parameter determination (atmospheric models, lines, and broadening, to name a few). The second one is, roughly speaking, data quality. The latter is dominated by S/N (see Table 1), which can make uncertainties escalate to higher values as S/N decreases. However, if S/N is high enough, any calculation is driven by the methodology employed to derive stellar parameters ([Recio-Blanco et al. 2006](#)). In Fig. 1, we plot uncertainties on T_{eff} and $[M/H]$ as a function of S/N, for all the spectra analysed. We assumed that our uncertainties behave as $\alpha e^{\frac{\beta}{S/N}}$. Using least squares, we can calculate α , which corresponds to the minimum uncertainty. We obtain 49K and 0.04 dex as lower limits to this method (assuming that S/N tends towards ∞).

In addition, our internal errors can tell us if a result is well defined or not. This is specially important for points close to the grid limits. We imposed the condition that a point is good only if its $1-\sigma$ levels fall within the limits of our grids. This removes spurious results close to the grid edges, which can lead to low-precision stellar atmospheric parameters.

Another important point is how to combine calculations coming from two different atmospheric model grids. We do not find a significant systematic offset between KURUCZ and MARCS models above 4000 K. However, as we clearly show in Fig. 2, an offset is noticeable for T_{eff} below 4000 K. This offset must be taken with care, since at low T_{eff} , the differences raise linearly and up to 100K. This shows an important issue regarding on how stellar atmospheric models were calculated. MARCS atmospheric models for $15 M_{\odot}$ were computed using spherical geometry. In spite of that fact, if we were to average those differences they will be at most 50K in the worst case scenario². Therefore, our internal uncertainties are compatible with that systematic effect. Global differences show a small average value of 8 ± 22 K. Thus, our final results are an average of KURUCZ and MARCS calculations, whenever both grids produce a well defined set of stellar atmospheric parameters for a given individual spectrum. For $[M/H]$ we obtained a small difference of 0.05 ± 0.02 dex, indicating that $[M/H]$ is very stable regardless of the model grid employed for the calculations.

There are stars in our sample with more than one spectrum taken in the same epoch (i.e. within two nights of each other). We calculated the parameters separately for each spectrum available. Then, we combined the results for spectra of the same star in the same epoch, calculating their average T_{eff} and $[M/H]$ weighted by the S/N of the spectra.

² We are in no position to state which atmospheric models are better. Of course, it can be argued that MARCS models are spherical; KURUCZ models, however, cover a wider atmospheric extension. Each approximation has its own assumptions, and unfortunately we have to deal with them in a reasonable manner.

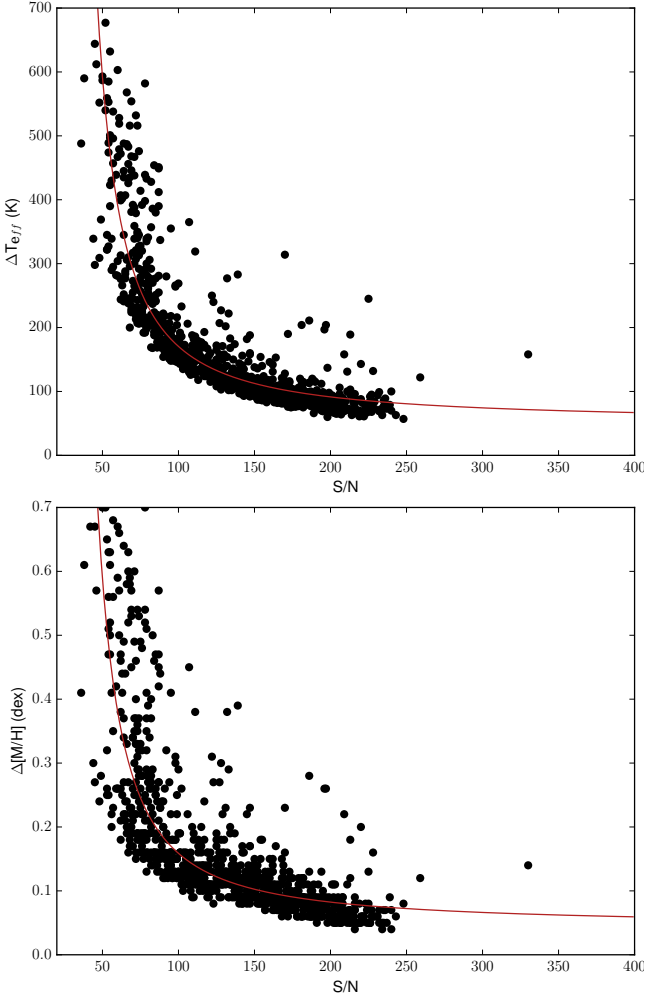


Figure 1. Derived ΔT_{eff} and $\Delta[M/H]$ against S/N. The data plotted are the results obtained for all the individual spectra in our sample, without taking into account that some stars have multiple spectra. The red line represents the fit to the behaviour of uncertainties as described in Sect. 3.3.

The histograms of the results are shown in Fig. 3. We did not combine spectra from different epochs of the same star in these figures because a large number of CSGs present spectral variability (see Paper II, for details). We also obtained the internal uncertainties for both temperature and metallicity. For this we used all the spectra of stars which do not show spectral variability. In the case of variable targets, as the variations typically have periods of hundreds of days, we compared spectra only inside each epoch. We obtained an internal dispersion of 25 K for T_{eff} , and 0.06 dex for $[M/H]$. These values are well below our internal uncertainties, thus proving that our method is stable when deriving stellar parameters of the same object in different epochs as long as it is not variable in SpT. We discuss the effects caused by SpT variability in detail in Sect. 4.1.3.

In order to evaluate the effect of fixing the value of microturbulence, we calculated two other sets of stellar parameters by varying microturbulence by $\pm 0.5 \text{ km s}^{-1}$ (see Figs. A2 and A3). Metallicities only vary by a factor of approximately ∓ 0.2 dex for the MARCS grid and ∓ 0.18 dex

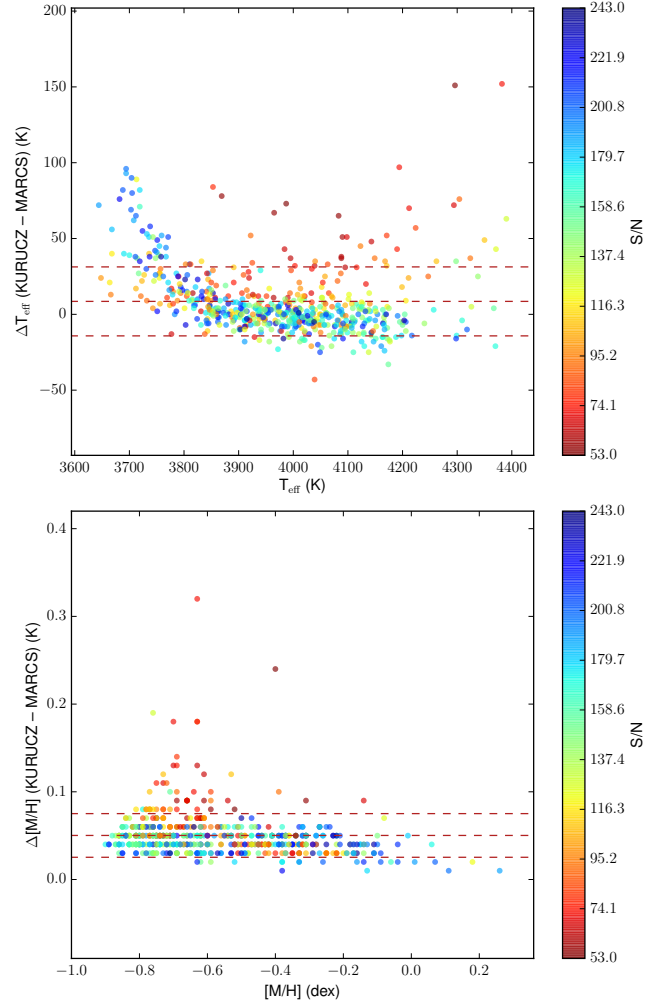


Figure 2. T_{eff} and $[M/H]$ differences when calculated using either KURUCZ or MARCS atmospheric models against combined values. All data plotted are the results obtained for all the individual spectra in our sample, even if they belong to the same star in the same epoch. Red dashed lines depict the average difference value and the $1\text{-}\sigma$ levels.

for the KURUCZ grid. However, the effective temperature was stretched by a small percentage: $\mp 15\%$ for MARCS, and $\mp 5\%$ for KURUCZ. The variations found do not alter any tentative temperature scale, since any correlation that we may want to calculate is scale-invariant.

Our derived average $[M/H]$, weighted by the S/N of each individual spectrum in our sample (i.e. including duplicated observations), is -0.35 ± 0.15 dex for the LMC, and -0.75 ± 0.11 dex for the SMC. Davies et al. (2015) made a careful and detailed compilation of literature values for each MC. They reported an average present-day metallicity range from -0.2 to -0.4 dex for the LMC, whereas the SMC ranges from -0.5 dex to -0.8 dex. These values are representative of what can be found in the literature (see Davies et al. 2015, and references therein). Thus, our results are fully consistent with what previous studies have found for each cloud, taking into account that Davies et al. (2015) mention that these typical values of $[M/H]$ for each MC are dependent on the sample included in each study.

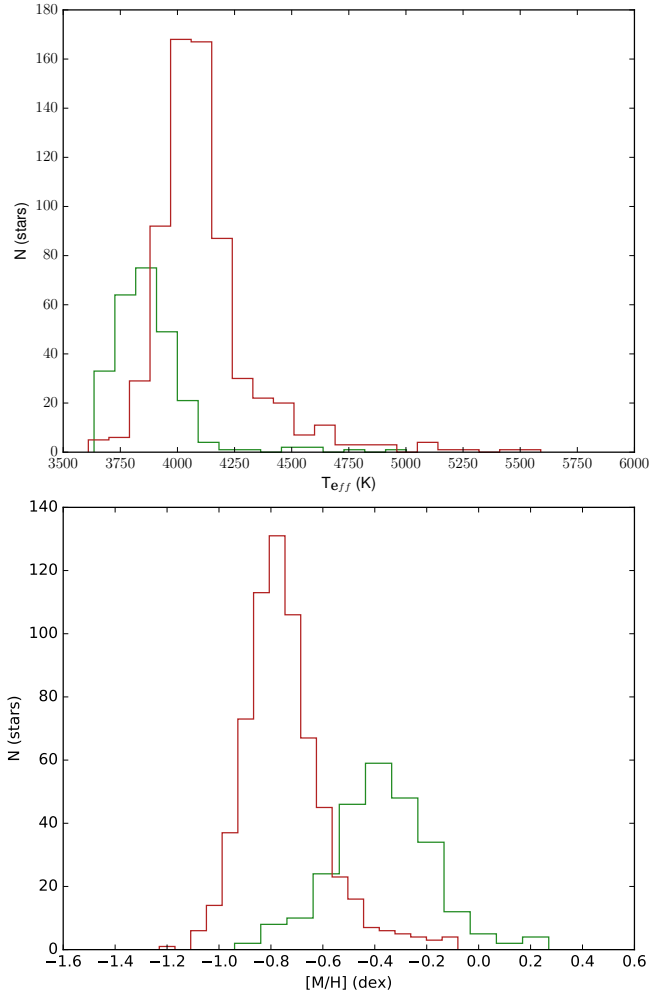


Figure 3. Derived T_{eff} and $[M/H]$ for the whole sample. LMC stars are plotted in red, whereas SMC stars are represented by a green line. The bin size was determined using the [Freedman & Diaconis \(1981\)](#) rule. The data obtained for spectra of the same star in different epochs are not combined, but treated as different stars for these figures.

3.4 LTE systematics

Our calculations are purely based on an LTE classical but conservative approach. Some recent works have made use of NLTE corrections to LTE calculations (e.g. [Davies et al. 2015](#); [Gazak et al. 2015](#); [Patrick et al. 2016](#)). To estimate the validity of our results, we need to know the systematics of our LTE calculations against NLTE methods. NLTE corrections for RSGs have been quantified in the literature for some chemical elements: Fe I, Ti I ([Bergemann et al. 2012](#)), Si I ([Bergemann et al. 2013](#)), and Mg I ([Bergemann et al. 2015](#)).

To accomplish this particular aim, we downloaded the spectra analysed by [Davies et al. \(2013, 2015\)](#), which are available under ESO program 088.B-0014(A). As there were multiple spectra for each star, we chose only those with $R \approx 7000$, of which there is only one per star. We chose this resolution because it is closest to that of our own sample. For consistency, we did not use those stars that had not been observed at this resolution. Then we applied our anal-

ysis to the same region of the *I*-band spectrum that we have used for our sample, as explained in previous sections. Before this, we also calculated our own RV for the stars, using the CaT spectral range, in the same way as for the sample of this work (see [Paper I](#)). In [Table 2](#) and [Fig. 4](#) we show a comparison between both methodologies. We obtain an average difference in $T_{\text{eff}} = -168 \pm 177$ K. For $[M/H]$ the offset is 0.00 ± 0.17 dex. Thus, our analysis results in lower effective temperatures and similar metallicities, see [Fig. 4](#). However, this comparison must be taken with care. Even though we assume that NLTE is a better approximation than LTE, the differences found are compatible with zero if we simply consider the standard deviation. To evaluate its statistical significance, we employed a BIC analysis (bayesian information criterion) to the T_{eff} difference. The result of this analysis is $\Delta\text{BIC} = \text{BIC}(\text{offset}) - \text{BIC}(\text{no offset}) = 1.77$. Thus, since ΔBIC is less than 2, we cannot ascertain that the difference between the NLTE and LTE temperatures is statistically significant, at least for this small comparison sample.

Our line diagnostics are dominated by Ti I and Fe I. [Bergemann et al. \(2012\)](#) reported that NLTE corrections for Ti I can be really important (up to 0.4 dex), whereas, NLTE Fe I corrections are smaller, reaching at most 0.15 dex. Si I NLTE corrections ([Bergemann et al. 2013](#)) are at a level similar to those of Fe I. Mg I also presents similar effects as Fe I and Si I ([Bergemann et al. 2015](#)). All these works ([Bergemann et al. 2012, 2013, 2015](#)) report that global $[M/H]$ calculations (as those presented here) can be affected at the level of $\Delta [M/H] \approx 0.15$ dex. Additionally, they also study the effects of NLTE on line profiles. As one might expect, line cores are more affected. Line cores form in the upper levels of the atmosphere, where the LTE approximation starts to deviate from “reality”, this effect can be seen in [Fig. A1](#) for only two lines. Our best fits are off for some lines around 8800Å because the LTE approach does not hold for the upper layers of the stellar atmosphere. However, our internal uncertainties are sufficiently conservative to account for any possible differences (see [Table 1](#)).

4 DISCUSSION

4.1 The temperature scale of the Magellanic cool supergiants

4.1.1 Correlations between effective temperature and spectral type

The large size of our sample allows us to study the T_{eff} scale drawn by CSGs in the MCs with an unprecedented statistical significance. We used the sample described in [Paper II](#), which comprises data from 2012 (SMC) and 2013 (LMC). It does not include any observations from earlier epochs (2010 and 2011). Firstly, we cannot combine many spectra from different epochs, given the spectral variability we detected. Secondly, essentially all the stars from the 2010 and 2011 runs were also observed in 2012 and 2013 and thus we are not losing any stars, while preventing duplicities. In total, there are 527 CSGs observed in these two epochs. Unfortunately, for some stars we do not present any stellar parameters. We discarded stars later than M3, as well as those for which we do not find good stellar parameters, according to the criterion given in [Sect. 3.3](#). In total we characterized

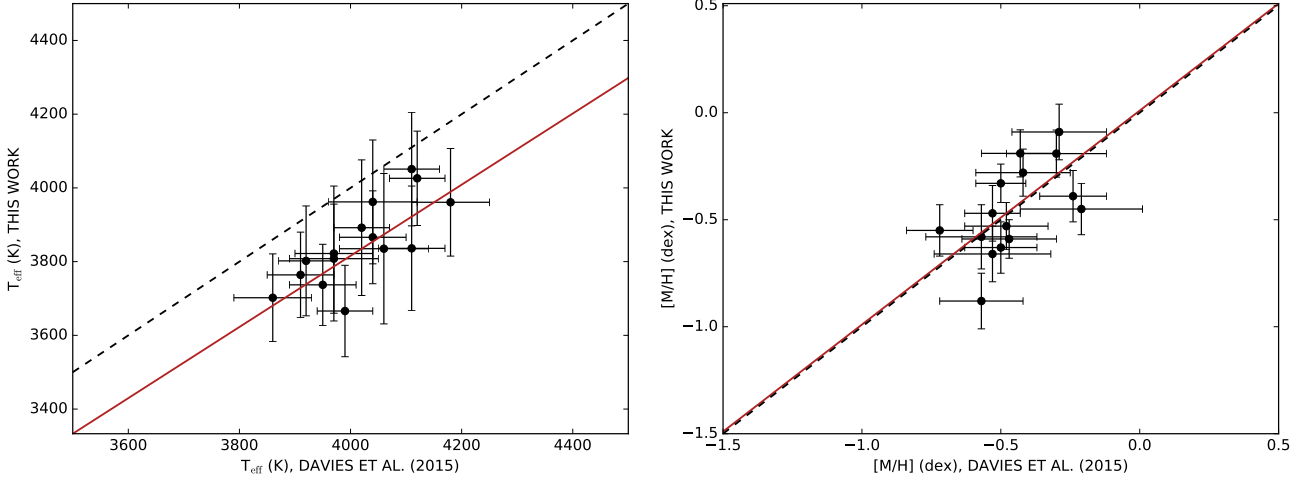


Figure 4. Our stellar atmospheric parameters vs those analysed by Davies et al. (2015). The dashed line represents a 1:1 relation, whereas the solid line is simply a linear fit through the points.

Table 2. Our calculations using the X-shooter spectra analysed by Davies et al. (2013, 2015). The names and stellar parameters of these stars are those used in Davies et al. (2015) (Dav15), but they are referred to the catalogue of Massey (2002). The STEPAR parameters are those obtained in the present work.

NAME	Galaxy	T_{eff} (STEPAR)	[M/H] (STEPAR)	T_{eff} (Dav15)	[M/H] (Dav15)
064048	LMC	3702 ± 119	-0.28 ± 0.11	3860 ± 70	-0.42 ± 0.17
067982	LMC	3764 ± 116	-0.19 ± 0.11	3910 ± 60	-0.43 ± 0.14
116895	LMC	3737 ± 110	-0.19 ± 0.11	3950 ± 60	-0.30 ± 0.18
131735	LMC	4051 ± 154	-0.33 ± 0.09	4110 ± 50	-0.50 ± 0.09
137818	LMC	3666 ± 124	-0.63 ± 0.12	3990 ± 50	-0.50 ± 0.13
143877	LMC	3835 ± 204	-0.09 ± 0.13	4060 ± 80	-0.29 ± 0.17
011709	SMC	3892 ± 184	-0.47 ± 0.13	4020 ± 50	-0.53 ± 0.10
020133	SMC	3808 ± 148	-0.45 ± 0.12	3970 ± 80	-0.21 ± 0.22
021362	SMC	3822 ± 183	-0.58 ± 0.15	3970 ± 70	-0.57 ± 0.20
030616	SMC	3866 ± 126	-0.59 ± 0.09	4040 ± 60	-0.47 ± 0.17
034158	SMC	3961 ± 146	-0.53 ± 0.11	4180 ± 70	-0.48 ± 0.15
035445	SMC	3962 ± 168	-0.66 ± 0.13	4040 ± 80	-0.53 ± 0.21
049478	SMC	3836 ± 169	-0.39 ± 0.12	4110 ± 60	-0.24 ± 0.12
050840	SMC	3802 ± 149	-0.55 ± 0.12	3920 ± 50	-0.72 ± 0.12
057386	SMC	4026 ± 128	-0.88 ± 0.13	4120 ± 50	-0.57 ± 0.15

445 CSGs, which represent 84% of the sample contained in Paper II (see Table A2).

Our sample covers a broad range in SpT (from G0 till M3) thus allowing us to ascertain the existence of a temperature scale. To this aim, we calculated the correlation coefficients of Pearson (r) and Spearman (r_s) between SpT and T_{eff} . While r is sensible to linear correlations, r_s is more robust and can manage non-linear correlations, if any. We computed r and r_s for each MC alone and for both galaxies together. To propagate uncertainties, we used a Monte Carlo method. We created 10 000 artificial samples of the same size as our own sample. Each artificial datapoint (i.e. an T_{eff} and SpT pair) in a generated sample was calculated by drawing it randomly from a two dimensional normal distribution centred on the values of one of the original measurements with a width given by the known uncertainties in each variable. Once these random samples were generated for all of our measurements, we calculated the correlation coefficients (r and r_s) for each one of the 10 000 realizations, and analysed their distribution. The final values are the averages of the correlations coefficients found for the 10 000 artificial

samples and their uncertainties are given by their standard deviation. The results of this process can be seen in Table 3.

The values of r and r_s obtained from our original sample indicate that SpT and T_{eff} are strongly correlated for CSGs, at least in the case of the MCs. The Montereale-calculated r and r_s remain similar to those of the original sample, in most cases both being inside the $2\text{-}\sigma$ interval. These results confirm the existence of the correlation, even when our relatively high uncertainties in T_{eff} are taken into account.

The trend drawn by the LMC population alone appears to be nearly linear (see Fig. 5b), because r is higher than r_s . It might be argued that the LMC correlation can arise from the presence of a few G supergiants far from the core of the SpT distribution. The G supergiants of the LMC do not seem to correspond to the same population as the K and M supergiants, contrarily to the YSGs from the SMC (Paper II). Thus, there is a strong reason to study the correlation coefficients for the LMC without the G supergiants. As there are only six G-stars in the LMC sample, the sample size is not significantly affected by removing them. We find that for the original sample, r clearly decreases (see Ta-

Table 3. Pearson (r) and Spearman (r_s) coefficients obtained for the correlations between T_{eff} and SpT in different subsamples. The values marked as Montecarlo are the average values and the standard deviations obtained from the 10000 samples generated through Montecarlo (see text for details). Some subsamples were limited by spectral type or by M_{bol} (see text for a detailed explanation).

Sample	From Montecarlo		Original sample		Size of the sample
	$r \pm \sigma_p$	$r_s \pm \sigma_s$	r	r_s	
SMC	-0.771 ± 0.022	-0.76 ± 0.03	-0.771	-0.82	257
LMC	-0.888 ± 0.013	-0.855 ± 0.021	-0.888	-0.811	188
LMC (K–M types)	-0.789 ± 0.024	-0.78 ± 0.03	-0.789	-0.79	182
Both MCs	-0.852 ± 0.011	-0.854 ± 0.013	-0.852	-0.914	445
SMC ($M_{\text{bol}} < -6$ mag)	-0.782 ± 0.023	-0.77 ± 0.03	-0.783	-0.81	212
SMC ($M_{\text{bol}} < -6.7$ mag)	-0.76 ± 0.03	-0.74 ± 0.04	-0.76	-0.79	140
LMC ($M_{\text{bol}} < -6$ mag)	-0.887 ± 0.014	-0.850 ± 0.023	-0.888	-0.803	165

ble 3), although the correlation still remains highly significant. Interestingly, r_s is nearly unaltered. When Montecarlo calculated coefficients are considered, both r and r_s decrease, although the difference between them becomes smaller. This behaviour is indicative of non-linearity ($r_s \gtrsim r$), which in turn is not unexpected. The T_{eff} scale of Levesque et al. (2006) was indeed not linear, possessing different slopes for K and M supergiants. The non-linearity seems less noticeable when G supergiants are included, because they have a very high weight on r due to their extreme positions in relation to the main cluster of points.

In the original SMC sample and in the combined MC sample, r_s is significantly higher than r . As we discussed earlier for the LMC, this indicates an underlying non-linearity in the T_{eff} scale. The Montecarlo-calculated coefficients, by contrast, are very similar. However, the fact that r_s and r are equal is still indicative of non-linearity because r_s is less sensitive than r . The break in linearity for the LMC sample seems to be located around the change between K and M types (Levesque et al. 2006). For the SMC, instead, the trend between SpT and T_{eff} seems to change around K0 (see Fig. 5a). Therefore, the slope of the T_{eff} scale appears to be different for G and K CSGs, as it seems to be different between K and M supergiants. SMC CSGs present a significant dispersion in T_{eff} for types earlier than K1. However, all the points above the main trend (for $T_{\text{eff}} > 4500$ K) correspond to low values of S/N (between 30 and 60). Thus, these points are not as trustworthy as those below them (see Fig. 1).

In all the cases studied, the correlation coefficients derived show that the SpT sequence is strongly related to T_{eff} . This result is in perfect agreement with the empirical results already presented in Paper II, where we explored the relation between SpT and T_{eff} using EW(Ti I) to connect them. In addition, we also found a significant but mild correlation between SpT and M_{bol} when mid- to high-luminosity CSGs (Ia and Iab) are considered (see sects. 3.2 and 4.1.1 from Paper II). The correlation coefficients between SpT and M_{bol} for subsamples of stars brighter than a given value of M_{bol} lay between -0.17 and -0.53 (see table 2 from Paper II). The SpT– T_{eff} coefficients for the whole SMC and LMC samples (Table 3) are significantly higher than the SpT– M_{bol} coefficients found in Paper II. If we apply the same cuts in luminosity used in Paper II to explore the SpT– M_{bol} correlation, the correlation coefficients between T_{eff} and SpT do not vary significantly (Table 3). These results confirm the conclusions of Paper II: SpT depends mainly on T_{eff} , though it has a weaker, second-order relation to M_{bol} .

4.1.2 New temperature scales

The results found in Sect. 4.1.1 imply a well-defined T_{eff} scale. Our next step is to describe this scale. Levesque et al. (2006) found that each galaxy seems to have its own temperature scale. In other words, RSGs from different galaxies having the same T_{eff} should present different SpTs. Therefore, each MC temperature scale must be considered separately. We derived an average T_{eff} and a standard deviation for each subtype, weighting each point by its corresponding S/N, within each galaxy. In this manner, we gave less weight to CSGs with larger uncertainties in T_{eff} . We present all these values for each SpT in Table 4 and in Fig. 6, to ease the comparison with fig. 9 of Levesque et al. (2006).

When we examine the typical T_{eff} for each SpT in each MC, we find that, in general terms, the values are compatible. For early G stars, there are significant discrepancies between the typical T_{eff} 's of each galaxy. However, the number of CSGs with these SpTs in both MCs is too low to consider this result as statistically meaningful. This applies as well to the subtype M3, where a significant difference is found, but there is only one star of this type in the SMC, and its spectrum has a low S/N. We found small discrepancies in the typical T_{eff} of each galaxy for subtypes K5 and M0. These differences are significant at $1\text{-}\sigma$, but not at the $2\text{-}\sigma$ level. Moreover, they are derived from a low number of CSGs from the SMC. Since we find no significant differences between the typical T_{eff} 's of adjacent SpTs (i.e. K3, K4, M1, or M2), we cannot interpret these small differences in K5 and M0 as an indication of two different SpT scales. Instead, our results are compatible with the existence of a unique T_{eff} scale followed by all CSGs, regardless of their metallicity. In this scenario, metallicity would only determine the typical SpTs, or in other words, which part of the T_{eff} scale is populated by the CSGs.

Using our data, the T_{eff} scales for the two MCs are not distinguishable (in statistical terms), which suggests a unique scale. However, this interpretation should be examined with care. The overlap between the two SpT distributions is very limited, and so any attempt to make a direct comparison between the LMC and SMC scales will be based on very few stars. We note that Levesque et al. (2006) studied the differences between CSGs from the Galaxy and the LMC, whose metallicities are different, without finding any significant differences between the corresponding T_{eff} scales, although the two galaxies have almost the same SpT coverage (the difference is only half a subtype in the samples of

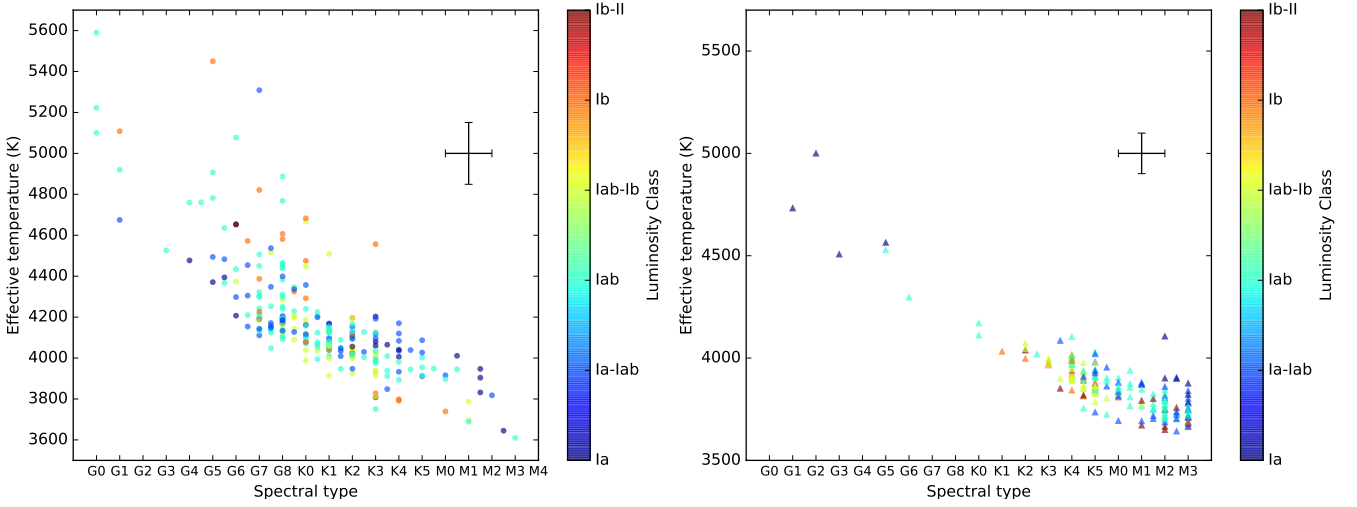


Figure 5. Effective temperature against spectral type. The colour indicates luminosity class. The black cross represents the median uncertainties. Both panels are on the same scale to make comparison easier. **Left (5a):** CSGs from the SMC. **Right (5b):** CSGs from the LMC.

Table 4. Effective temperature scale detailed for each subtype, for both MCs. For each SpT, the S/N weighted-mean of T_{eff} and its corresponding weighted standard deviation are shown (see Sect. 4.1.4 for further details)

SpT	SMC			LMC		
	Number	$\langle T_{\text{eff}} \rangle$ (K)	$\pm\sigma(T_{\text{eff}})$ (K)	Number	$\langle T_{\text{eff}} \rangle$ (K)	$\pm\sigma(T_{\text{eff}})$ (K)
G0	3	5516	± 169	–	–	–
G1	3	5081	± 99	1	4734	–
G2	–	–	–	1	5002	–
G3	1	4526	–	1	4509	–
G4	3	4503	± 82	–	–	–
G5	9	4657	± 417	2	4559	± 14
G6	12	4472	± 314	1	4299	–
G7	29	4202	± 147	–	–	–
G8	45	4202	± 125	–	–	–
K0	30	4135	± 134	2	4134	± 29
K1	34	4077	± 62	1	4034	–
K2	27	4059	± 65	5	4047	± 27
K3	27	4050	± 108	8	3988	± 61
K4	13	4024	± 91	43	3942	± 64
K5	7	3976	± 57	35	3886	± 68
M0	5	3942	± 57	16	3840	± 52
M1	6	3856	± 81	17	3790	± 60
M2	2	3802	± 51	33	3785	± 97
M3	1	3610	–	22	3751	± 54

Levesque et al. 2006). Moreover, we find a somewhat high dispersion of T_{eff} in each SpT. This is not unexpected. In addition to intrinsic uncertainties, there are many physical effects contributing to this dispersion: variations in luminosity by more than one order of magnitude within each subtype, implying large changes in the extension of the atmospheres; variations in mass-loss rate that affect the structure of the molecular envelope; variations in metallicity within each galaxy, and so on. The average value of the T_{eff} dispersions ($\sigma(T_{\text{eff}})$), weighted by the number of stars in each SpT, is 100 K for the SMC and 48 K for the LMC. As the difference in T_{eff} between SpTs is only a few tens of Kelvin, for K and M types, it is likely that small samples would result in a non-meaningful scale due to the stochastic effects emerging from incomplete statistics.

Although we have observed almost all the stars used by Levesque et al. (2006), we prefer not to compare their T_{eff} 's individually because of the possibility of spectral variability, which might imply changes in T_{eff} . Therefore, we simply compare our T_{eff} scale with those obtained by Levesque et al. (2006). For late K to early M CSGs, our scale covers a narrower range of T_{eff} 's when compared to Levesque et al. (2006). Interestingly, while for early K types our scales seem fully compatible, below late K we derived significantly higher T_{eff} 's. These results are only statistically significant for the LMC samples, as the number of M RSGs from the SMC is almost negligible. This systematic difference is likely related to our different ways to calculate T_{eff} 's. While we obtained the T_{eff} from spectral synthesis of photospheric weak metallic lines, Levesque et al. (2006) employed the shape of

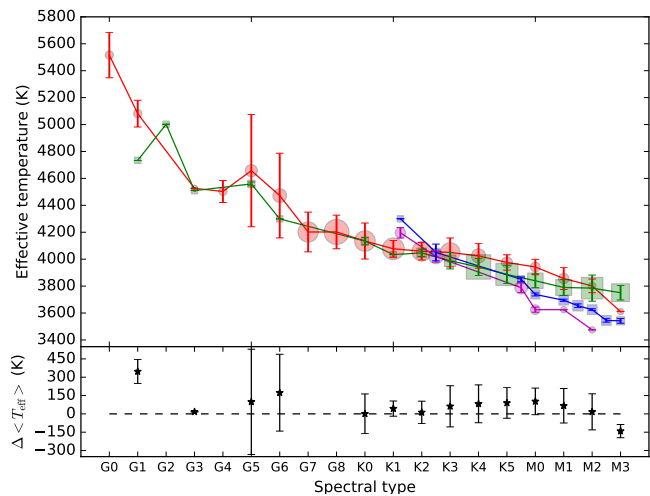


Figure 6. **Upper panel:** Effective temperature scale for our samples of CSGs from the SMC (red) and the LMC (green). We also overplotted the temperature scale derived by [Levesque et al. \(2006\)](#) for the SMC (purple) and the LMC (blue). The size of the symbols is proportional to the number of CSGs that contribute to each point. The absence of a symbol for a given SpT indicates that there are not CSGs with that SpT. The coloured error bars indicate the S/N-weighted standard deviation of the CSGs of the corresponding SpT. Note that for the SMC, the error bars lie inside the symbols in most cases. The exact values used for this figure are detailed in Table 4. **Lower panel:** Differences (SMC–LMC) between the mean values of the effective temperature of each MC at each SpT. The differences have not been calculated for SpTs that are absent in one of the galaxies. The uncertainties are the sums of the corresponding standard deviations.

their whole spectral range (from 4000Å to 9500Å), which is fully dominated by TiO bands for late K and M subtypes. As [Davies et al. \(2013\)](#) demonstrated, using the TiO bands results in cooler temperatures than found when employing atomic lines. Finally, we point out that, although ([Davies et al. 2013](#)) did not find a T_{eff} scale, our temperatures for K and M CSGs fall within the T_{eff} range of 4100 ± 150 K where they place all RSGs, except for the spectral types M2 and M3, which correspond to slightly lower temperatures. Our method uses atomic lines to calculate the T_{eff} and our sample has a high statistical weight. Therefore we can safely expect our T_{eff} scale to be a better representation of photospheric temperatures than those in previous works based on TiO bands.

4.1.3 Spectral variability and effective temperature

In [Paper II](#) we analysed the spectral variability of our sample, using multi-epoch data for approximately a hundred stars from each MC that had showed significant changes in their spectral type ($\Delta_{\text{v}}\text{SpT}$) between epochs. We found that spectral changes were accompanied by variations in spectral features generally assumed to respond to T_{eff} , but not by variations in features that respond to luminosity. Now, we can test directly the relation between $\Delta_{\text{v}}\text{SpT}$ and $\Delta_{\text{v}}T_{\text{eff}}$. For this, we used the same procedure as in [Paper II](#): we took all the stars observed in more than one epoch and tagged as variable (i.e., exhibiting a change larger than our typical

Table 5. Pearson (r) and Spearman (r_s) coefficients obtained for the variables indicated. The coefficients marked as Montecarlo are the means and the standard deviations obtained from the 10000 samples generated through a Montecarlo process (see text for details).

Variables		From Montecarlo		Original sample	
X	Y	$r \pm \sigma_p$	$r_s \pm \sigma_s$	r	r_s
$\Delta_{\text{v}}\text{SpT}$	$\Delta_{\text{v}}T_{\text{eff}}$	-0.68 ± 0.03	-0.65 ± 0.04	-0.68	-0.62
$\Delta_{\text{v}}\text{SpT}$	$\Delta_{\text{v}}[\text{M}/\text{H}]$	-0.04 ± 0.06	-0.03 ± 0.06	-0.04	-0.02
$\Delta_{\text{v}}T_{\text{eff}}$	$\Delta_{\text{v}}[\text{M}/\text{H}]$	0.25 ± 0.05	0.24 ± 0.05	0.25	0.27

error for SpT, one subtype, between any two given epochs) and computed differences in SpT and T_{eff} from one epoch to the other. When more than two epochs are available, we calculated the differences between all the possible epoch combinations (see Fig. 7).

As done for the correlation between SpT and T_{eff} , we obtained the Pearson (r) and Spearman (r_s) correlation coefficients for $\Delta_{\text{v}}\text{SpT}$ versus $\Delta_{\text{v}}T_{\text{eff}}$. Again, we did this for the original data and for 10000 samples generated through a Montecarlo process, such as that explained in Sect. 4.1.1. The results of this process are shown in Table 5. Both correlation coefficients, r and r_s , reveal the existence of a significant correlation. The significance is similar, though higher, than for the correlation obtained between $\Delta_{\text{v}}\text{SpT}$ and $\Delta_{\text{v}}\text{EW}(\text{Ti I})$ found in [Paper II](#), where the latter was used as proxy for T_{eff} . As a sanity check, we also calculated the correlation coefficients of $\Delta_{\text{v}}[\text{M}/\text{H}]$ with $\Delta_{\text{v}}\text{SpT}$ and $\Delta_{\text{v}}T_{\text{eff}}$ (see Table 5). In the case of $\Delta_{\text{v}}[\text{M}/\text{H}]/\Delta_{\text{v}}\text{SpT}$, all correlation coefficients are compatible with zero, as expected (see Fig. 7a). This not only confirms that our methodology does not introduce spurious correlations, but also provides an independent check that our calculations produce a non-skewed [M/H]. In the case of $\Delta_{\text{v}}[\text{M}/\text{H}]/\Delta_{\text{v}}T_{\text{eff}}$ (see Fig. 7b), we found a weak correlation that corresponds to the degeneracy between T_{eff} and [M/H]. Degeneracy between stellar parameters has been studied in the literature, as for example in [Schönrich & Bergemann \(2014\)](#) and [Ting et al. \(2017\)](#). In particular [Ting et al. \(2017\)](#) show very clearly the effects of parameter degeneracy in their figure 15. Thus, the degeneracy we found between T_{eff} and [M/H] is not unexpected at all. Indeed [Ting et al. \(2017\)](#) find that degeneracy between these two parameters in the same sense as found in this work is unavoidable and to a large degree independent of spectral resolution. Degeneration is an intrinsic issue to any calculation, especially for cool stars. It is possible to minimize its effects, as we have done in this work by a careful choice of our diagnostic features. We mixed low χ_1^3 lines, which will depend strongly on T_{eff} , with some high χ_1 lines that will strongly depend on [M/H].

We thus find that not only there is a global correlation between SpT and T_{eff} for the sample as a whole, but also, when we consider the SpT changes of a given star, they correlate strongly to changes in T_{eff} . Does this $\Delta_{\text{v}}\text{SpT}/\Delta_{\text{v}}T_{\text{eff}}$ correlation imply that spectral variability is mainly driven by changes in T_{eff} ? We know that other factors affect SpT, and [Davies et al. \(2013\)](#) conclude that SpT in RSGs does

³ Lower level excitation potential

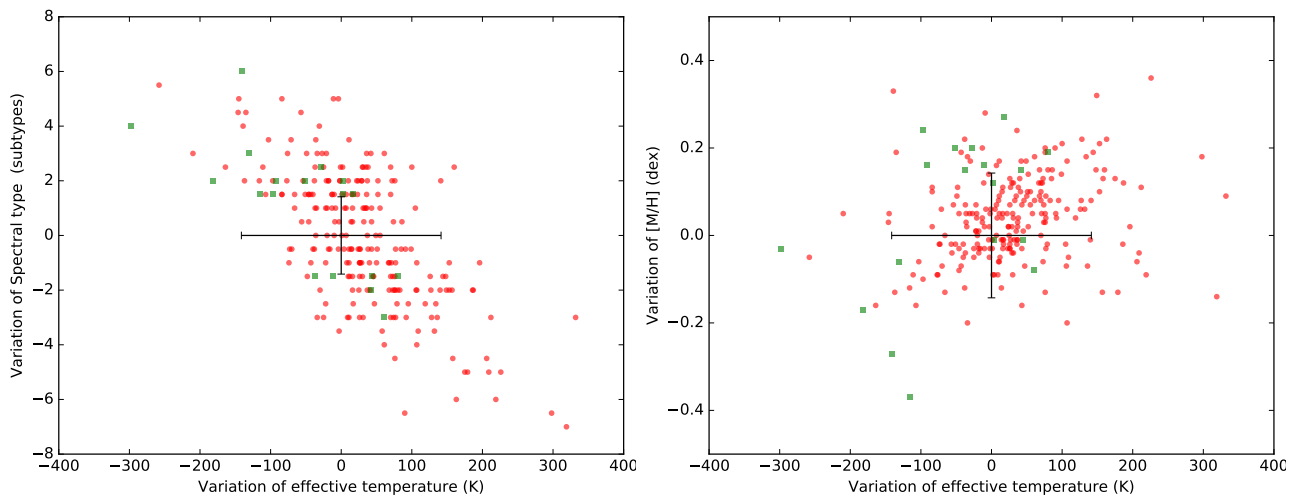


Figure 7. Variations in the effective temperature against variations in **Left (7a):** SpT and **Right (7b)** [M/H]. Each point is the difference between two epochs for a given supergiant. The colour indicates the SpT that the CSG changed to. Green squares are LMC CSGs; red circles are SMC CSGs. The black cross at (0,0) shows the median error in each axis. Epochs when a star changed to SpTs later than M3 are not used.

not only depend on T_{eff} . In view of the dispersion found in Fig. 5, we cannot disagree with this conclusion. Indeed, [Paper II](#) found a significant correlation between SpT and M_{bol} for the global sample, although this correlation is clearly weaker than that between SpT and T_{eff} . However, when we consider the changes in SpT of a given star, it seems to imply only variations in T_{eff} . The correlation of $\Delta_{\text{v}}\text{SpT}$ with the variations in lines sensitive to surface gravity (features classically used for luminosity classification) is nonexistent ([Paper II](#)). Moreover, despite the intrinsic degeneracy between $\Delta_{\text{v}}[\text{M}/\text{H}]$ with $\Delta_{\text{v}}T_{\text{eff}}$, the correlation between $\Delta_{\text{v}}\text{SpT}$ and $\Delta_{\text{v}}[\text{M}/\text{H}]$ is still compatible with 0, a result expectable if $\Delta_{\text{v}}\text{SpT}$ is not affected by spurious effects in our calculations. Although there could be other physical properties, beyond surface gravity, that may have a significant impact on $\Delta_{\text{v}}\text{SpT}$, but they are unlikely to be the main driver of changes in SpT. In view of all this, even though the SpT of an RSG does not only depend on T_{eff} , we have to conclude that spectral variations are, to a large extent, driven by changes in T_{eff} , regardless of other second order effects. This conclusion reinforces the idea advanced in Sect. 4.1.1: although SpT is sensitive to luminosity, it is a second order effect when compared to the dependence on T_{eff} . The fact that this dependence on luminosity is seen when we consider the whole sample, but does not appear when we study the variations of a given star supports the idea that it is related to evolutionary process, as suggested by [Beasar & Davies \(2016\)](#).

4.1.4 The typical temperatures of cool supergiants

In previous sections we have shown that a strong correlation exists between SpT and T_{eff} . In addition, we have failed to find a statistically significant difference between the T_{eff} scales of the LMC and the SMC. On the other hand, the two MCs have different typical metallicities and different SpT distributions, as we already showed in [Paper II](#). Here we want to test if there is indeed a significant difference between the T_{eff} distributions from different environments.

Table 6. Fraction of rejections of the null hypothesis of the KST (at $\alpha = 0.02$) done over pairs of T_{eff} distributions from each MC, for different-size subsamples. The rejection of the null hypothesis means that the samples of each MC are considered as significantly different. The fractions were calculated over groups of 10000 subsamples randomly taken. The size refers to the number of targets in the subsample of each MC. We provide as uncertainties of our fractions the $2\text{-}\sigma$ confidence intervals, which are equal to $1/\sqrt{n}$, where $n = 10000$. The limited tag refers to our sample restricted to RSGs (K and M SpTs) of mid to high luminosity (Ia to Iab). See text for details.

Size of the sample	Fraction of rejections of the null hypothesis	
	Not limited	Limited
5	0.00 ± 0.01	0.00 ± 0.01
7	0.19 ± 0.01	0.12 ± 0.01
10	0.30 ± 0.01	0.19 ± 0.01
15	0.71 ± 0.01	0.54 ± 0.01
20	0.96 ± 0.01	0.89 ± 0.01
25	0.99 ± 0.01	0.95 ± 0.01
50	1.00 ± 0.01	1.00 ± 0.01

We compared our samples from the LMC and the SMC using a Kolmogorov-Smirnov Test (KST). We required a level of significance $\alpha = 0.02$ to reject the null hypothesis (both samples are indistinguishable), finding that the KST rejected the null hypothesis for our samples by a wide margin. For stronger confirmation, we calculated through a Montecarlo process 10000 random samples of the size of our original sample for each galaxy, by allowing each star to take random values of its effective temperature according to a gaussian distribution. After this, we passed pairs of these samples (one from each galaxy) through the KST. The null hypothesis was rejected for all cases. Under the light of this result, we can conclude that the T_{eff} distribution of CSGs is significantly different between the two galaxies.

Our results appear to be contradictory with conclusions of [Davies et al. \(2013\)](#), who argued that all CSGs have roughly the same T_{eff} . They based this conclusion on the fact

that they could not find significant differences between the typical T_{eff} of their RSG samples from the two MCs. Successive works by the same group have supported this conclusion for other CSG populations. At this point, we have to remark that our results do not imply in any manner that the values of T_{eff} calculated through their methods are incorrect. In fact, we have showed in Sect. 3.4 that the values obtained through our methods are statistically indistinguishable from theirs, at least for the small sample that we could use for the comparison. Under the light of our results, we can speculate that their conclusion, as well as successive confirmations given in later works, is a consequence of two effects combined: the limited size of their samples and the dispersion in T_{eff} that we find within each subtype (see Sect. 4.1.4 and Fig. 4). In order to confirm this assertion, we devised the following test: we randomly took subsamples of different sizes. For each different subsample size, we took 10000 random subsamples from each MC. Then, we applied the KST (at $\alpha = 0.02$) to each of the 10000 pairs of subsamples (one from each galaxy). Finally, we calculated the fraction of the 10000 pairs of subsamples of a given size for which the null hypothesis (both subsamples are statistically indistinguishable) was rejected. Results are provided in Table 6; they clearly indicate that, whenever small subsamples are taken, the null hypothesis cannot be rejected with confidence. As the sample size increases, the fraction of rejection increases. By the time a sample size reaches 50 CSGs, from each galaxy, the null hypothesis is rejected in all experiments. Contrariwise, with the sample sizes of Davies et al. (2015), the null hypothesis cannot be rejected in most experiments.

It could be argued that our samples are not fully equivalent to those of Davies et al. (2015), because we include a large number of G stars and also low luminosity CSGs (Ib and Ib-II). Therefore, we repeated our calculations using only RSGs (K and M types) of mid to high luminosity (Ia and Iab luminosity classes). This restriction has the added advantage that we also avoid the systematic difference between the LMC and SMC samples at low luminosities, caused by the difference in distance modulus (0.5 mag) between the two galaxies. As can be seen in Table 6, the rejections become even lower for small samples. However, as in the non-limited subsamples case, for sizes of 50 CSGs the rejections reach 100%.

4.2 Metallicity effects

In the previous section we concluded that CSGs in the SMC present a significantly different T_{eff} distribution from those in the LMC. This difference, also reflected in their SpT distribution, is believed to be a consequence of the difference in typical metallicity (Elias et al. 1985). In fact, evolutionary models (Ekström et al. 2012; Georgy et al. 2013) predict a shift in the lowest T_{eff} that CSGs can reach during their evolution due to metallicity. Previous works obtained contradictory results in this matter. On one hand, Drout et al. (2012) analysed 189 RSGs from the galaxy M33. They found that the T_{eff} distribution of RSGs seems to change for different galactocentric radius (see fig. 22 of Drout et al. 2012), which implies different typical metallicities. On the other hand, Gazak et al. (2015) studied a sample of 27 RSGs from the galaxy NGC 300. Although they obtained a clear trend between the galactocentric distance of the RSGs and their

metallicity (see their fig. 6), in good agreement with previous works, they did not find a clear correlation between metallicity and T_{eff} (see their fig. 7).

In Fig. 8, we represent our values of T_{eff} and [M/H] for all the stars in our sample. As can be seen, the distribution of CSGs in each MC occupies different positions in the diagram. However, there is no clear correlation within the sample of each galaxy. To test statistically if there is a noticeable trend in the [M/H] span within each galaxy, we calculated the correlation coefficients (r and r_s). We used the same methodology as in Sect. 4.1.1. The results are shown in Table 7.

The coefficients for the LMC are very low, close to non-significant. Instead, for the SMC there is a weak correlation. However, in both cases the sign is the opposite to that expected, in the sense that we find higher T_{eff} 's at higher metallicities. This result is a direct consequence of the presence of G CSGs. In the case of the LMC, as explained above, these stars are not part of the same population as RSGs. For the SMC, the problem is the presence of many G supergiants with low S/N, as can be seen in Fig. 8a. To avoid this last effect, we repeated all our calculations imposing a lower limit on $S/N \geq 100$. The results are also shown in Table 7. A weak correlation persists for the LMC objects, because its G CSGs present mid to high S/N, but in the case of the SMC the correlation simply disappears. Finally, we wanted to calculate again the correlation for the LMC but only including K and M RSGs. Moreover, to allow a more direct comparison with the works of Drout et al. (2012) and Gazak et al. (2015), we calculated the correlation only for the subsample of luminous RSGs (i.e. K and M types only and luminosity classes Ia and Iab only). With these limits, the LMC presents a weak correlation with the expected sign. Instead, for the SMC there is not a significant correlation, as in the case of the cut in S/N because the G CSGs were most of the stars with low S/N.

From all these results, we conclude that there is not a noticeable correlation between [M/H] and T_{eff} among the CSGs of each galaxy. This result has an interesting contrast with the fact that CSGs from the SMC are less metallic than those from the LMC, but also significantly cooler. We can advance two possible reasons why we do not find any significant correlation within each galaxy. Firstly, we found average $[M/H]_{\text{LMC}} = -0.33 \pm 0.20$ dex and $[M/H]_{\text{SMC}} = -0.73 \pm 0.17$ dex. The standard deviation within each population is not very high (≈ 0.2 dex) when compared to the difference $[M/H]_{\text{LMC}} - [M/H]_{\text{SMC}}$ (0.40 dex). Secondly, the existence of significant spectral variability (especially among the SMC sample) can blur away any correlation, because a star of a given [M/H] may present very different T_{eff} 's depending on the observation moment. As variability is more frequent in the SMC sample, this effect may explain why we find a weak correlation for the LMC sample, but not for that from the SMC. Under these assumptions the results of Gazak et al. (2015) are not entirely unexpected. Although their sample spans a range of 0.6 dex, its standard deviation is only 0.14 dex, i.e. even smaller than the dispersions of our MC samples. Unfortunately, Drout et al. (2012) do not provide values of metallicity for their sample. Thus, a similar analysis is not possible for their work.

The idea that the typical SpT of a population is related to its metallicity stems from the comparative study of a few

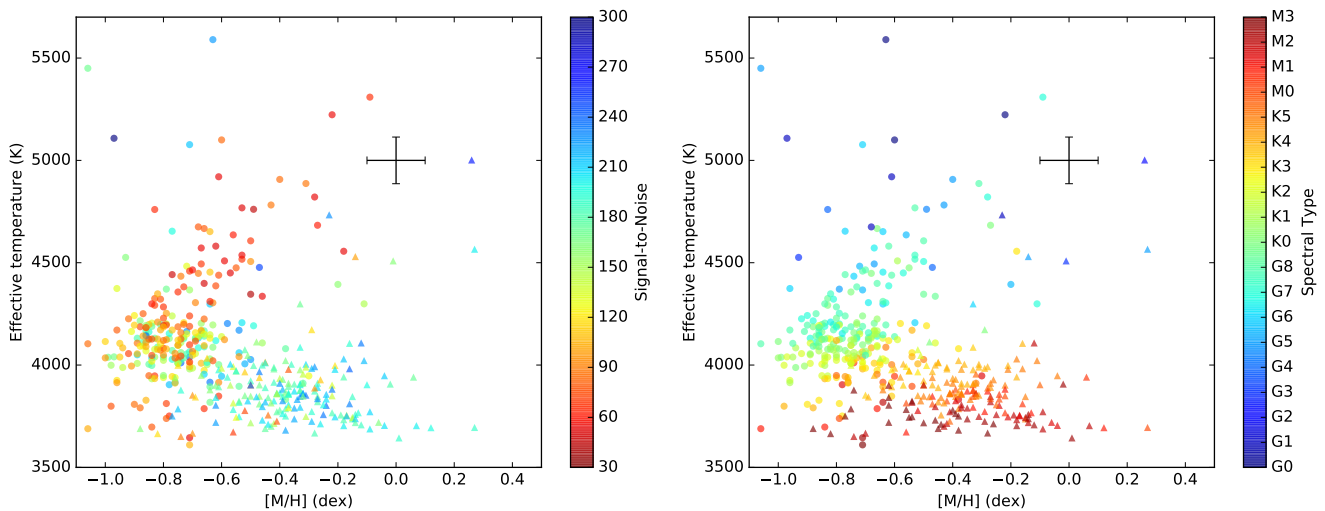


Figure 8. Effective temperature against Metallicity for CSGs from both, the SMC (circles) and the LMC (triangles). The black cross represents the median uncertainties. **Left (8a):** The color indicates the S/N. **Right (8b):** The color indicates the SpT.

Table 7. Pearson (r) and Spearman (r_s) coefficients obtained for the correlations between T_{eff} and $[M/H]$ in different subsamples from both MCs. Some subsamples were limited to $S/N > 100$ or to include only luminous RSGs (those having K or M types and Ia or Iab luminosity classes). The coefficients tagged as Montecarlo are the means and the standard deviations obtained from the 10000 samples generated through Montecarlo (see text for details).

Sample	From Montecarlo		Original sample		Size of the sample
	$r \pm \sigma_p$	$r_s \pm \sigma_s$	r	r_s	
SMC	0.35 ± 0.05	0.33 ± 0.06	0.35	0.25	257
LMC	0.18 ± 0.06	0.11 ± 0.06	0.18	-0.06	188
SMC ($S/N > 100$)	-0.04 ± 0.07	-0.03 ± 0.07	-0.04	-0.02	155
LMC ($S/N > 100$)	0.15 ± 0.06	0.08 ± 0.07	0.15	-0.11	175
SMC (RSGs)	0.07 ± 0.07	0.07 ± 0.08	0.07	0.08	137
LMC (RSGs)	-0.19 ± 0.08	-0.18 ± 0.07	-0.19	-0.17	152

populations (Levesque & Massey 2012). Our results seem to confirm warmer temperatures at lower $[M/H]$, as the population in the SMC is clearly warmer than that in the LMC. However, the idea that there is a smooth functional relation between typical T_{eff} and $[M/H]$ is an unproven extrapolation, perhaps suggested by the behaviour of theoretical tracks. Our results do not provide evidence in this sense. In fact, despite the significant difference in $[M/H]$ between the RSGs from the LMC and those from our Galaxy, the average SpT difference appears to be at most one subtype (Elias et al. 1985; Levesque 2013), which is almost unnoticeable. Therefore, it cannot be translated into a very large difference in T_{eff} . For example, in Levesque et al. (2006) the difference between the LMC and the Milky Way is not significant at all (only 15 K). In view of this, the existence of a smooth correlation between the typical temperature of CSGs and metallicity must be kept on hold until further tests can be performed.

4.3 Comparison with evolutionary tracks

We calculated absolute bolometric magnitudes for our CSGs in Paper II. Using the T_{eff} 's calculated in this work, we can plot our CSGs in the Hertzsprung-Russel diagram. In

Figs. 9 and 10 we compare our data to Geneva evolutionary tracks. We used them to illustrate the state-of-the-art theoretical evolutionary tracks because they are widely employed within the literature. Although there are other tracks available (e.g. Brott et al. 2011), they are qualitatively similar to those of Geneva and the range of T_{eff} 's covered is also very similar (see Paper II).

Unfortunately, Geneva tracks for the LMC typical metallicity are not available. Instead, we provide the evolutionary tracks for solar metallicity ($Z = 0.014$) to help in the interpretation of the figures. The evolutionary tracks for the LMC typical metallicity should fall between those for SMC and Solar metallicities.

Firstly, we must remark that the samples plotted are biased towards hot temperatures, because all stars with types later than M3 have been discarded from our analysis. Given the SpT- T_{eff} correlation we found, we should expect them to have lower temperatures. In addition, several CSGs from our sample were discarded because they reach the edges of our synthetic spectra grids (see Sect. 3.3). Therefore, there should be many more CSGs with lower temperatures than those shown, specially in the case of the LMC. Any interpretation of the figures must take this bias into consideration. Secondly, for clarity we do not represent tracks with rota-

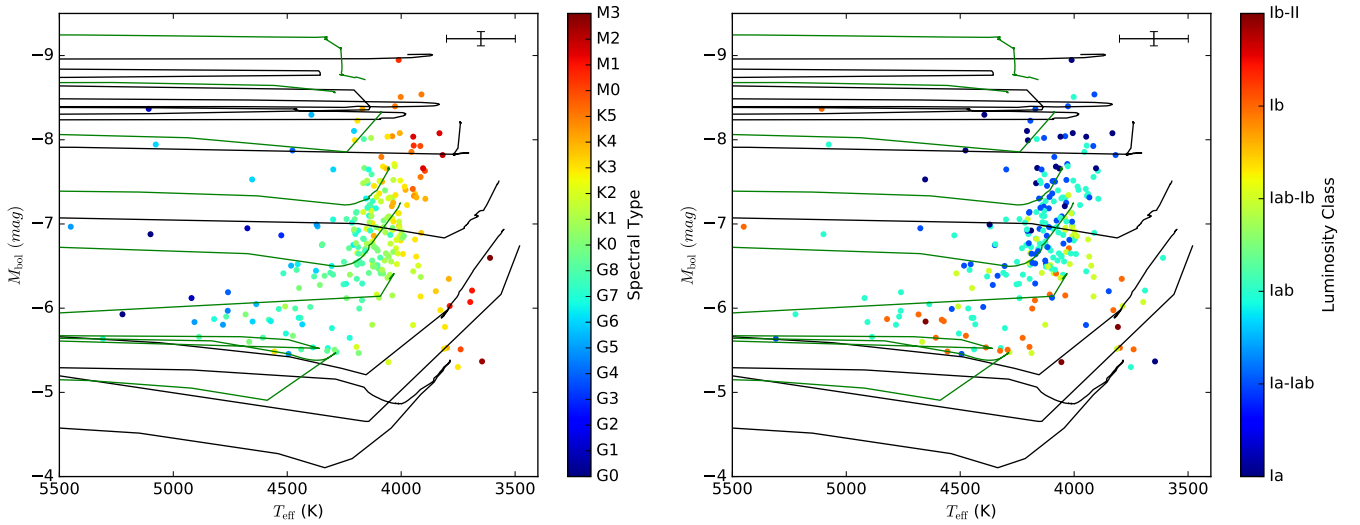


Figure 9. Our sample of CSGs from the SMC, plotted together with Geneva evolutionary tracks. Green tracks are for the typical metallicity of the SMC (Georgy et al. 2013). Black tracks are for Solar metallicity (Ekström et al. 2012). The tracks shown correspond (for both metallicities), from bottom to top, to stars of 9, 12, 15, 20, 25, and $32 M_{\odot}$. The black cross represents the median uncertainties. **Left (9a):** The color indicates the spectral types of the sample. **Right (9b):** The color indicates the Luminosity classes of the sample.

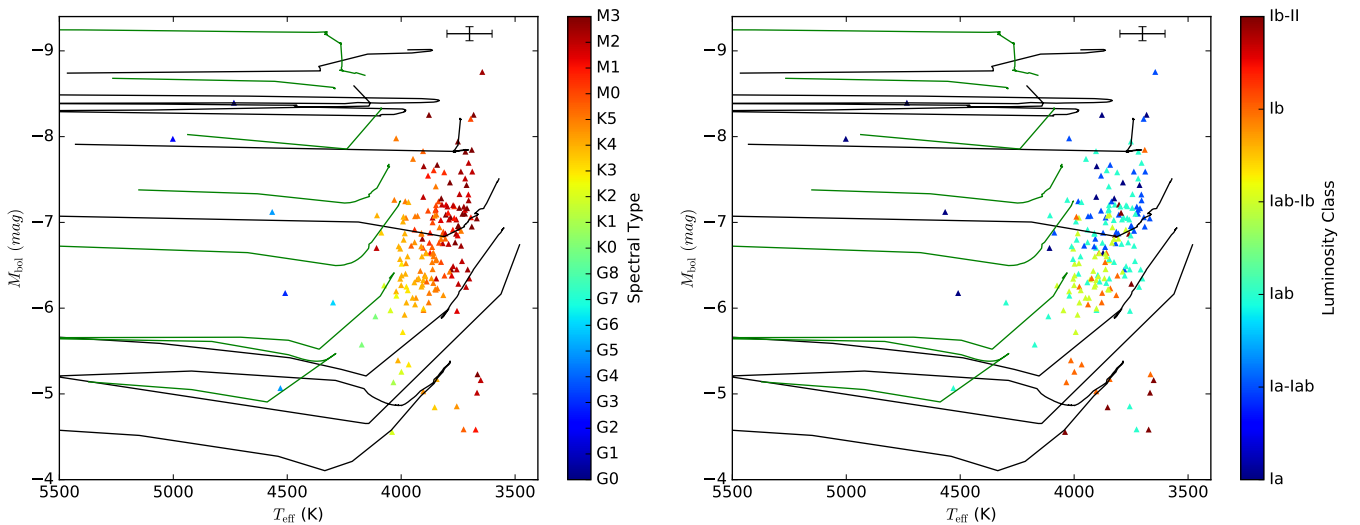


Figure 10. Our sample of CSGs from the LMC (excluding objects with spectral type M3 and later), plotted together with Geneva evolutionary tracks. Symbols are as in Fig. 9. No tracks for LMC metallicity are available. Note that the sharp cut at low temperatures is almost certainly an artefact of our sample selection and procedure. **Left (10a):** The color indicates the spectral types of the sample. **Right (10b):** The color indicates the Luminosity classes of the sample.

tion. The main effect of rotation is an increase in the predicted luminosity for each track. For most, it does not affect substantially the lowest temperature reachable. The change is only noticeable for the tracks with the highest masses, where we do not have almost any CSG. Therefore, the effect of rotation does not impact our analysis.

In the case of the SMC (Fig. 9), the overall agreement with our results and the evolutionary tracks is good. CSGs with luminosities between $M_{\text{bol}} \sim -6.5$ mag and $M_{\text{bol}} \sim -7.5$ mag present temperatures compatible with the evolutionary tracks. This group represents most of the SMC sample. However, there are two groups of CSGs with

$T_{\text{eff}} < 4000$ K that are clearly colder than any T_{eff} shown in the evolutionary tracks at any given luminosity for the SMC. One group is formed by CSGs less luminous than $M_{\text{bol}} \sim -6.5$ mag. Some of these CSGs present the lowest temperatures in the SMC sample. In fact, these low luminosity CSGs reach temperatures as low as those predicted for Solar metallicity. The other group are stars brighter than $M_{\text{bol}} \sim -7.5$ mag with moderately low T_{eff} . The presence of these highly luminous CSGs, with temperatures lower than those predicted, was noticed in previous works (e.g. Levesque et al. 2007; Davies et al. 2013). As the lowest T_{eff} reachable by a CSG is theoretically connected to its metallicity, we

checked the metallicities of these stars. The $[M/H]$ of all but three is inside the typical values of the SMC sample. Thus, it seems that metallicity cannot explain their lower temperatures. Furthermore, [Davies et al. \(2013\)](#) discussed the assumptions made for treatment of convection used to generate the evolutionary tracks. Interestingly, they mention that the locations of these cool CSGs could be moved to cooler or warmer temperatures if the assumptions regarding convection are modified.

For the LMC (Fig. 10), the comparison is more problematic. Geneva evolutionary tracks of high-mass stars are not available for the typical $[M/H]$ of the LMC. Consequently, we can only employ the tracks for SMC and solar metallicities to evaluate the behaviour of stars. Most LMC CSGs have T_{eff} values within the range displayed by the evolutionary tracks. However, many stars, especially among those more luminous than $M_{\text{bol}} \lesssim -7$ mag present T_{eff} values expected for solar metallicity, or even slightly lower. Again, those stars are not much more metallic than the typical values of our LMC sample. Moreover, as we explained above, we must take into account that there must be many RSGs with even lower T_{eff} 's that are not included in our plot.

From our analysis of both MCs, we found that the agreement between evolutionary tracks and our sample is, in general terms, good. However, there are CSGs with lower temperatures than those present in the evolutionary tracks. Some of them are low luminosity CSGs and seem to correspond to the evolutionary track of $9M_{\odot}$. Therefore, although their spectral morphologies correspond to supergiants, they may be in fact highly luminous red giants. During the AGB phase, hot bottom burning may increase the luminosity of massive giants even above the classical limit of $M_{\text{bol}} = -7.1$, thus mimicking the behaviour of more massive stars (e.g. [Ventura et al. 2000](#)) However, we can say very little about this group, given that our sample is highly incomplete at such low luminosities.

Most of the CSGs with T_{eff} lower than those of evolutionary tracks in both MCs are concentrated at high luminosities. These CSGs have especially late spectral types and, as can be seen in fig. 19 of [Paper II](#), they present the highest mass-loss rates in both galaxies. The luminosity of these CSGs is compatible with evolutionary tracks for $\geq 20 M_{\odot}$. It is tempting to think that these high-mass tracks have a problem with their minimum T_{eff} . Moreover, the evolutionary tracks for these high masses predict that CSGs do not stay at the coolest edge of the track for long, but instead return quickly back to warmer T_{eff} . However, there is another possibility, which we already advanced in [Paper II](#). Mid-luminosity CSGs might perhaps evolve towards higher luminosities and lower T_{eff} 's than predicted by $\sim 12\text{--}15M_{\odot}$ evolutionary tracks. If so, they would form a group of CSGs with luminosities typical of higher initial masses ($M_{\text{bol}} \lesssim -7$ mag). Recent results by [Beasor & Davies \(2016\)](#) support this scenario. They found that, while most RSGs in the LMC cluster NGC 2100 present luminosities between $\log(L/L_{\odot}) \sim 4.5$ ($M_{\text{bol}} \sim -6.5$ mag) and $\log(L/L_{\odot}) \sim 4.8$ ($M_{\text{bol}} \sim -7.3$ mag), there are two RSGs with significantly higher luminosities: $\log(L/L_{\odot}) > 4.95$ ($M_{\text{bol}} \lesssim -7.6$ mag). Unfortunately, as our sample does not represent a coeval population we cannot verify this scenario. Even then, our data show that there is a substantial number of CSGs with stellar atmospheric parameters inconsistent with current evolutionary tracks.

Therefore, it is necessary to find an explanation for such high-luminosity CSGs inside the evolutionary theory of high-mass stars.

5 CONCLUSIONS

In this work, we have obtained stellar atmospheric parameters (T_{eff} and $[M/H]$) for the largest homogeneous sample of CSGs belonging to the MCs. For this, we used spectral features found in the CaT spectral range observed at mid-resolution. The results of the present manuscript are summarized below:

(i) We compare our results to NLTE calculations using the sample observed by [Davies et al. \(2015\)](#), and find a small systematic difference. This difference is not significant given our internal uncertainties, but this result should be contrasted with a larger sample.

(ii) We find a significant correlation between T_{eff} and SpT. This correlation is much stronger than that between SpT and M_{bol} . We also find a significant correlation when we analyse the variations of SpT and T_{eff} . Therefore, we conclude that SpT is mainly driven by T_{eff} , although luminosity has some influence on it.

(iii) From the correlations described above, we conclude that there is a meaningful temperature scale for CSGs. This scale seems to be the same for stars in the two MCs. At least, given our level of precision, we cannot tell any difference between the scales found for the two MCs. Although more studies are needed, our results seem to indicate that all CSGs belonging to the MCs are on a similar T_{eff} scale.

(iv) Although the samples of both MCs seem to follow the same T_{eff} scale, we report a significantly different range of T_{eff} for each MC. This together with conclusion (ii), implies that the shift in the typical SpT of each galaxy is caused by the difference in T_{eff} .

(v) When we study the relation between $[M/H]$ and T_{eff} , we find that for the sample from the LMC, there is a weak correlation, and for that from the SMC there is no correlation at all. From these and other statistical analyses, we conclude that the relation between T_{eff} and $[M/H]$ is subtle, and unlikely linear. In consequence, the effect of $[M/H]$ on the T_{eff} distribution is only noticeable for samples with very different typical metallicities, as when CSG samples from the SMC and the LMC are compared to each other.

(vi) We compare our samples with Geneva evolutionary tracks. We find that the physical properties of mid-luminosity CSGs from both MCs, which represent the majority of our samples, match well the evolutionary tracks. However, most of the high-luminosity CSGs present temperatures significantly lower than expected from the evolutionary tracks. This result indicates that evolutionary tracks are not predicting correctly the nature of high-luminosity RSGs. Therefore, these stars require further research, both theoretical and observational.

ACKNOWLEDGEMENTS

The observations have been partially supported by the OPTICON project (observing proposals 2010B/01, 2011A/014

and 2012A/015), which is funded by the European Commission under the Seventh Framework Programme (FP7). Part of the observations have been taken under service mode (proposal AO171) and the authors gratefully acknowledge the help of the AAO support astronomers. This research is partially supported by the Spanish Government Ministerio de Economía y Competitividad under grants FJCI-2014-23001 and AYA2015-68012-C2-2-P (MINECO/FEDER). This research has made use of the Simbad database, operated at CDS, Strasbourg (France). This publication also made use of data products from the Two Micron All Sky Survey, which is a joint project of the University of Massachusetts and the Infrared Processing and Analysis Center/California Institute of Technology, funded by the National Aeronautics and Space Administration and the National Science Foundation.

REFERENCES

- Asplund M., Grevesse N., Sauval A. J., 2005, in Barnes III T. G., Bash F. N., eds, *Astronomical Society of the Pacific Conference Series Vol. 336, Cosmic Abundances as Records of Stellar Evolution and Nucleosynthesis*. p. 25
- Barklem P. S., Piskunov N., O'Mara B. J., 2000, *A&AS*, **142**, 467
- Beasar E. R., Davies B., 2016, *MNRAS*, **463**, 1269
- Bergemann M., Kudritzki R.-P., Plez B., Davies B., Lind K., Gazak Z., 2012, *ApJ*, **751**, 156
- Bergemann M., Kudritzki R.-P., Würl M., Plez B., Davies B., Gazak Z., 2013, *ApJ*, **764**, 115
- Bergemann M., Kudritzki R.-P., Gazak Z., Davies B., Plez B., 2015, *ApJ*, **804**, 113
- Bessell M. S., Wood P. R., 1984, *PASP*, **96**, 247
- Brott I., et al., 2011, *A&A*, **530**, A115
- Davies B., Kudritzki R.-P., Figer D. F., 2010, *MNRAS*, **407**, 1203
- Davies B., et al., 2013, *ApJ*, **767**, 3
- Davies B., Kudritzki R.-P., Gazak Z., Plez B., Bergemann M., Evans C., Patrick L., 2015, *ApJ*, **806**, 21
- Dorda R., González-Fernández C., Negueruela I., 2016b, *A&A*
- Dorda R., Negueruela I., González-Fernández C., Tabernero H. M., 2016a, *A&A*
- Drout M. R., Massey P., Meynet G., 2012, *ApJ*, **750**, 97
- Ekström S., et al., 2012, *A&A*, **537**, A146
- Ekström S., Georgy C., Meynet G., Groh J., Granada A., 2013, in Kervella P., Le Bertre T., Perrin G., eds, *EAS Publications Series Vol. 60, EAS Publications Series*. pp 31–41 ([arXiv:1303.1629](https://arxiv.org/abs/1303.1629)), doi:10.1051/eas/1360003
- Elias J. H., Frogel J. A., Humphreys R. M., 1985, *ApJS*, **57**, 91
- Freedman D., Diaconis P., 1981, *Zeitschrift für Wahrscheinlichkeitstheorie und Verwandte Gebiete*, **57**, 453
- García-Hernández D. A., García-Lario P., Plez B., Manchado A., D'Antona F., Lub J., Habing H., 2007, *A&A*, **462**, 711
- Gazak J. Z., Davies B., Kudritzki R., Bergemann M., Plez B., 2014, *ApJ*, **788**, 58
- Gazak J. Z., et al., 2015, *ApJ*, **805**, 182
- Georgy C., et al., 2013, *A&A*, **558**, A103
- González-Fernández C., Dorda R., Negueruela I., Marco A., 2015, *A&A*, **578**, A3
- Graczyk D., et al., 2014, *ApJ*, **780**, 59
- Gray R. O., Corbally C. J., 1994, *AJ*, **107**, 742
- Gustafsson B., Edvardsson B., Eriksson K., Jørgensen U. G., Nordlund Å., Plez B., 2008, *A&A*, **486**, 951
- Heiter U., Eriksson K., 2006, *A&A*, **452**, 1039
- Humphreys R. M., 1979, *ApJS*, **39**, 389
- Humphreys R. M., McElroy D. B., 1984, *ApJ*, **284**, 565
- Kupka F. G., Ryabchikova T. A., Piskunov N. E., Stempels H. C., Weiss W. W., 2000, *Baltic Astronomy*, **9**, 590
- Lee T. A., 1970, *ApJ*, **162**, 217
- Levesque E. M., 2013, in Kervella P., Le Bertre T., Perrin G., eds, *EAS Publications Series Vol. 60, EAS Publications Series*. pp 269–277 ([arXiv:1302.0822](https://arxiv.org/abs/1302.0822)), doi:10.1051/eas/1360031
- Levesque E. M., Massey P., 2012, *AJ*, **144**, 2
- Levesque E. M., Massey P., Olsen K. A. G., Plez B., Josselin E., Maeder A., Meynet G., 2005, *ApJ*, **628**, 973
- Levesque E. M., Massey P., Olsen K. A. G., Plez B., Meynet G., Maeder A., 2006, *ApJ*, **645**, 1102
- Levesque E. M., Massey P., Olsen K. A. G., Plez B., 2007, *ApJ*, **667**, 202
- Massey P., 2002, *ApJS*, **141**, 81
- Massey P., Olsen K. A. G., 2003, *AJ*, **126**, 2867
- Mészáros S., et al., 2012, *AJ*, **144**, 120
- Metropolis N., Rosenbluth A. W., Rosenbluth M. N., Teller A. H., Teller E., 1953, *J. Chem. Phys.*, **21**, 1087
- Meynet G., Maeder A., 2000, *A&A*, **361**, 101
- Patrick L. R., Evans C. J., Davies B., Kudritzki R.-P., Gazak J. Z., Bergemann M., Plez B., Ferguson A. M. N., 2015, *ApJ*, **803**, 14
- Patrick L. R., Evans C. J., Davies B., Kudritzki R.-P., Hénault-Brunet V., Bastian N., Lapenna E., Bergemann M., 2016, *MNRAS*, **458**, 3968
- Piskunov N. E., Kupka F., Ryabchikova T. A., Weiss W. W., Jeffery C. S., 1995, *A&AS*, **112**, 525
- Recio-Blanco A., Bijaoui A., de Laverny P., 2006, *MNRAS*, **370**, 141
- Ryabchikova T., Piskunov N., Kurucz R. L., Stempels H. C., Heiter U., Pakhomov Y., Barklem P. S., 2015, *Phys. Scr.*, **90**, 054005
- Schönrich R., Bergemann M., 2014, *MNRAS*, **443**, 698
- Skrutskie M. F., et al., 2006, *AJ*, **131**, 1163
- Tabernero H. M., Montes D., González Hernández J. I., 2012, *A&A*, **547**, A13
- Ting Y.-S., Conroy C., Rix H.-W., Cargile P., 2017, *ApJ*, **843**, 32
- Ventura P., D'Antona F., Mazzitelli I., 2000, *A&A*, **363**, 605
- Walker A. R., 2012, *Ap&SS*, **341**, 43

APPENDIX A: EXTRA MATERIAL

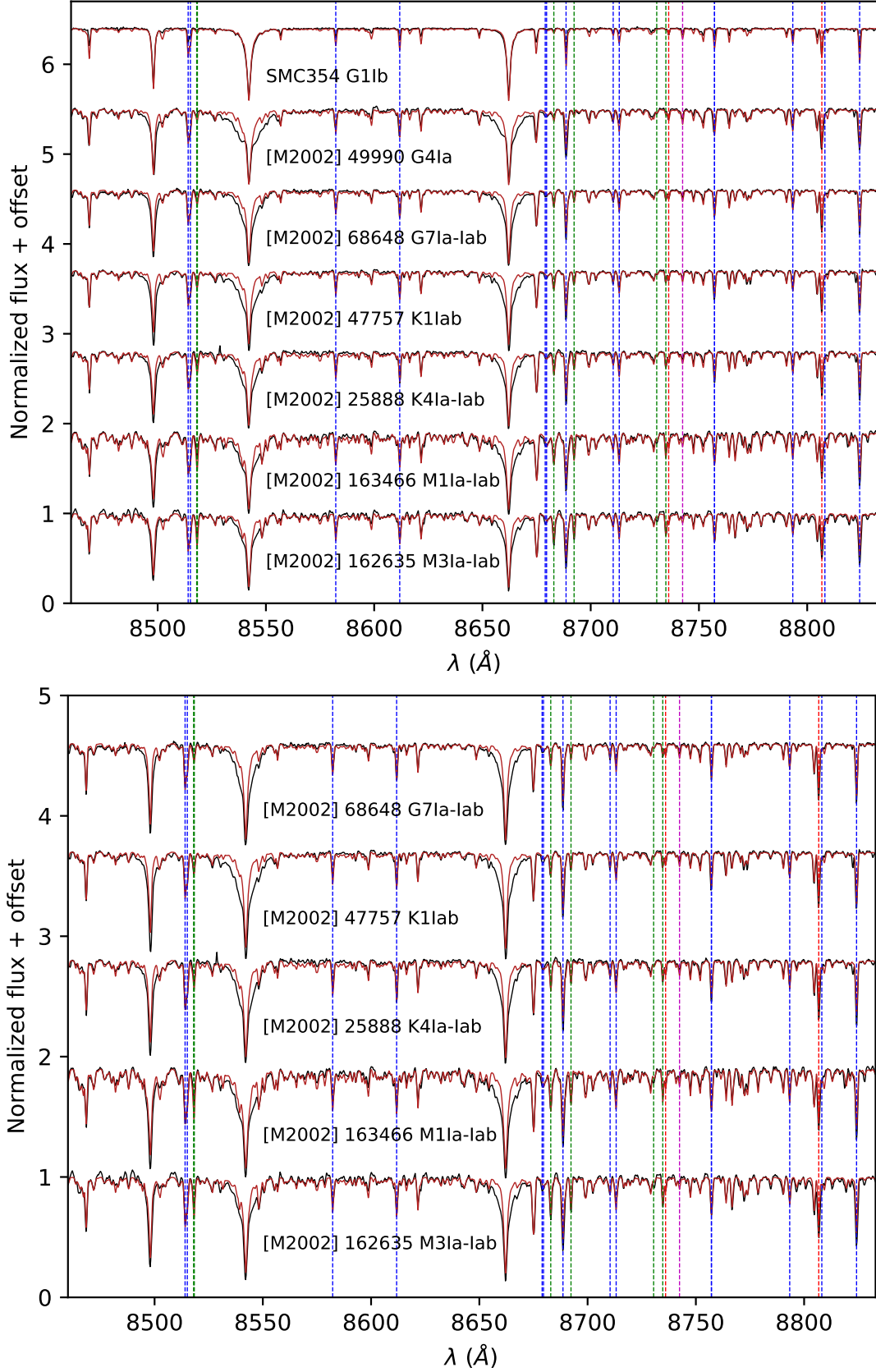
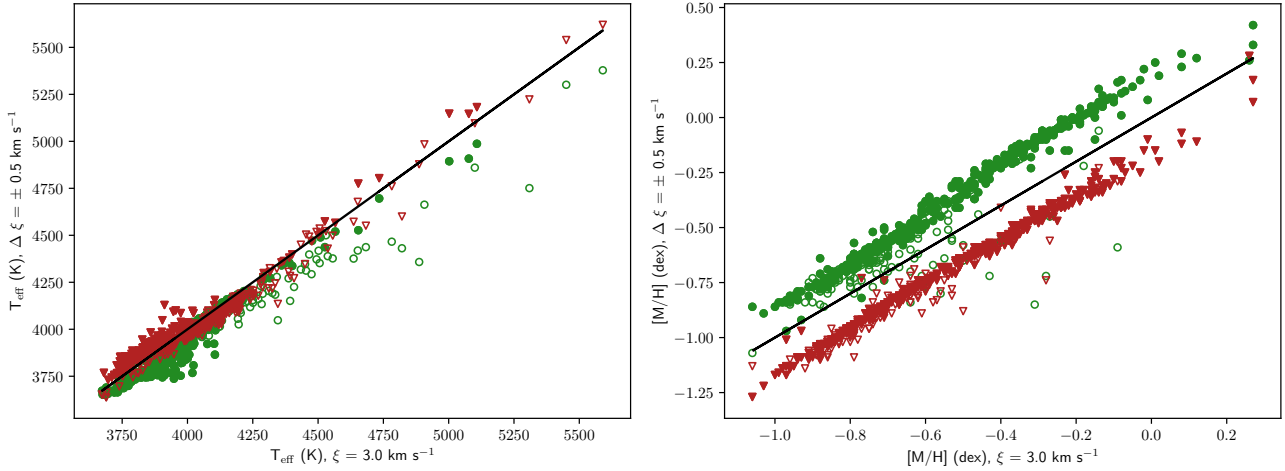


Figure A1. Best-fit synthetic spectra (red line) against observations (black line) for our two synthetic grids: **Upper panel (A1a)** (KURUCZ) and **Lower panel (A1b)** (MARCS). Dashed lines refer to the diagnostic lines (see Tab. A1) we employed in our calculations: Mg (red), Si (magenta), Ti (green), and Fe (blue).

Table A1. Lines used to derive stellar parameters, we show only predominant features on each spectral window.

Rank	λ interval (Å)	λ_{line} (Å)	Element	χ_{low} (eV)	log gf (dex)	log γ_6 /ABO data
1	8514.40 ± 1.90	8514.09	Fe I	2.20	-2.23	257.246
		8515.12	Fe I	3.01	-2.08	-7.77
2	8518.30 ± 1.50	8518.03	Ti I	2.13	-0.94	-7.80
		8518.35	Ti I	1.87	-1.05	-7.75
3	8582.35 ± 1.35	8582.26	Fe I	2.99	-2.13	-7.12
4	8611.80 ± 0.90	8611.80	Fe I	2.85	-1.93	312.264
5	8679.00 ± 2.10	8679.00	Fe I	6.02	-3.29	-7.13
		8679.63	Fe I	4.97	-1.29	-7.52
6	8682.90 ± 1.30	8682.98	Ti I	1.05	-1.79	283.246
7	8688.95 ± 1.65	8688.62	Fe I	2.18	-1.21	253.245
8	8692.00 ± 1.00	8692.33	Ti I	1.05	-2.13	-7.75
9	8711.50 ± 3.00	8710.18	Mg I	5.93	-0.54	–
		8710.39	Fe I	4.91	-0.54	-7.51
		8712.68	Mg I	5.93	-1.57	–
		8713.19	Fe I	2.94	-2.47	-7.50
10	8730.75 ± 0.95	8730.50	Ti I	3.35	-1.57	-7.75
11	8735.25 ± 1.75	8734.71	Ti I	1.05	-2.24	283.247
		8736.02	Mg I	5.94	-0.73	–
12	8742.25 ± 0.75	8742.45	Si I	5.87	-0.07	-7.33
13	8757.20 ± 1.60	8757.19	Fe I	4.26	-2.06	310.265
14	8792.85 ± 1.35	8793.34	Fe I	4.61	-0.09	-7.54
15	8806.00 ± 2.70	8806.76	Mg I	4.34	-0.13	530.277
		8808.17	Fe I	5.01	-1.08	-7.49
16	8824.36 ± 1.15	8824.22	Fe I	2.20	-1.54	254.245
17	8838.75 ± 1.25	8838.43	Fe I	2.86	-2.05	310.265

**Figure A2.** T_{eff} and $[M/H]$ calculated with two different microturbulent velocities ($\xi = 3 \pm 0.5 \text{ km s}^{-1}$) using KURUCZ synthetic spectra. Red triangles correspond to $\xi = 2.5 \text{ km s}^{-1}$, whereas green circles correspond to $\xi = 3.5 \text{ km s}^{-1}$. Open symbols represent stars with uncertainties on T_{eff} of 200 K or more.

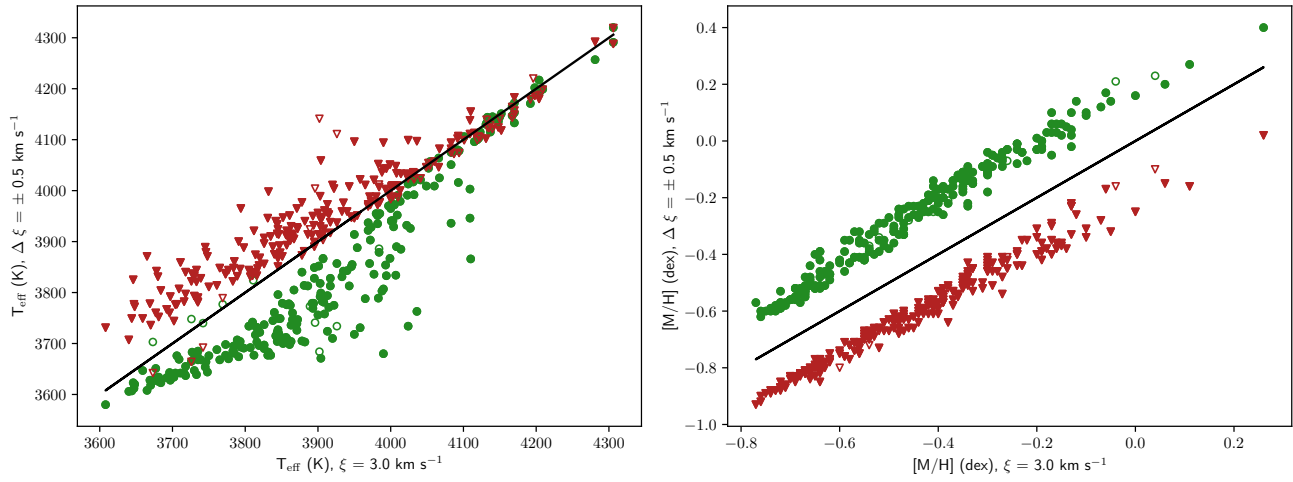


Figure A3. Same as Fig. A2 but for MARCS synthetic spectra calculations.

Table A2: A list of CSGs for which we derived stellar atmospheric parameters (T_{eff} and $[M/H]$). The SpT and the LC are taken from [Paper I](#), while the M_{bol} correspond to those from [Paper II](#). Stars tagged as variable are shown in different rows, one for each epoch (Variability is indicated at the column Var.). The epochs are: A=2010, B=2011, C=2012, D=2013.

ID	Cloud	RA J2000	DEC J2000	Var.	Epochs	T_{eff} (K)	ΔT_{eff} (K)	$[M/H]$ (dex)	$\Delta[M/H]$ (dex)	SpT	LC	M_{bol} (mag)
8324	SMC	00:47:16.86	-73:08:08.59	yes	B	4121	119	-0.94	0.14	K0	Ia-Iab	-6.88
8324	SMC	00:47:16.86	-73:08:08.59	yes	A	4237	307	-0.82	0.37	G7	Iab	-6.88
8324	SMC	00:47:16.86	-73:08:08.59	yes	C	4201	174	-0.79	0.19	G7	Iab	-6.88
8367	SMC	00:47:18.14	-73:10:39.32	yes	B	4011	77	-0.82	0.08	K2	Ia-Iab	-7.23
8367	SMC	00:47:18.14	-73:10:39.32	yes	A	3981	210	-0.73	0.19	K3.5	Ia	-7.23
8367	SMC	00:47:18.14	-73:10:39.32	yes	C	4139	123	-0.60	0.11	G8	Iab	-7.23
8930	SMC	00:47:36.89	-73:04:44.25	yes	B	4076	66	-0.59	0.07	K2.5	Ia-Iab	-7.82
8930	SMC	00:47:36.89	-73:04:44.25	yes	A	3778	209	-0.77	0.17	M3	Iab	-7.82
8930	SMC	00:47:36.89	-73:04:44.25	yes	C	3818	96	-0.64	0.08	M2	Ia-Iab	-7.82
9766	SMC	00:48:01.26	-73:23:37.56	no	A, B	3960	103	-0.81	0.10	K1.5	Iab-Ib	-7.11
10889	SMC	00:48:27.01	-73:12:12.10	yes	B	4121	95	-0.37	0.07	K2	Ia	-8.54
10889	SMC	00:48:27.01	-73:12:12.10	yes	A	3995	114	-0.43	0.09	K3.5	Ia	-8.54
10889	SMC	00:48:27.01	-73:12:12.10	yes	C	3911	99	-0.32	0.06	K5	Ia-Iab	-8.54
11101	SMC	00:48:31.95	-73:07:44.14	yes	B	3998	134	-0.84	0.13	K0	Iab-Ib	-6.98
11101	SMC	00:48:31.95	-73:07:44.14	yes	A	4036	148	-0.72	0.15	K0.5	Ia-Iab	-6.98
11101	SMC	00:48:31.95	-73:07:44.14	yes	C	4009	149	-0.67	0.13	K3.5	Iab	-6.98
11709	SMC	00:48:46.37	-73:28:20.99	no	A, B	4034	93	-0.53	0.08	K3.5	Ia-Iab	-7.81
11939	SMC	00:48:51.85	-73:22:39.78	yes	B	3931	76	-0.70	0.07	K5	Iab	-7.68
11939	SMC	00:48:51.85	-73:22:39.78	yes	A	3854	152	-0.74	0.14	M2	Ia-Iab	-7.68
11939	SMC	00:48:51.85	-73:22:39.78	yes	C	4080	91	-0.38	0.07	K3	Ia	-7.68
12322	SMC	00:49:00.33	-72:59:36.08	yes	B	4082	82	-0.49	0.08	K3	Ia	-8.04
12322	SMC	00:49:00.33	-72:59:36.08	yes	A	4086	144	-0.63	0.14	K3.5	Ia	-8.04
12322	SMC	00:49:00.33	-72:59:36.08	yes	C	3947	101	-0.30	0.06	M1.5	Ia	-8.04
12707	SMC	00:49:08.20	-73:14:15.89	yes	B	4147	165	-0.94	0.19	K0	Ia-Iab	-6.94
12707	SMC	00:49:08.20	-73:14:15.89	yes	A	4133	224	-0.82	0.24	K0.5	Ia-Iab	-6.94
12707	SMC	00:49:08.20	-73:14:15.89	yes	C	4093	150	-0.87	0.15	K2	Iab	-6.94
13472	SMC	00:49:24.53	-73:18:13.91	yes	A	4318	153	-0.39	0.16	G7	Ia-Iab	-8.30
13472	SMC	00:49:24.53	-73:18:13.91	yes	C	4394	79	-0.20	0.09	G5.5	Ia	-8.30
13740	SMC	00:49:30.40	-73:26:50.35	no	A, B, C	3936	77	-0.83	0.07	K2.5	Ib	-6.82
13951	SMC	00:49:34.40	-73:14:09.93	yes	B	4020	91	-0.71	0.09	K1.5	Ia-Iab	-7.22
13951	SMC	00:49:34.40	-73:14:09.93	yes	A	3996	146	-0.73	0.14	K2	Ia-Iab	-7.22
13951	SMC	00:49:34.40	-73:14:09.93	yes	C	3974	128	-0.66	0.11	K3	Iab	-7.22
15510	SMC	00:50:06.40	-73:28:10.85	no	A, B, C	3985	60	-0.64	0.05	K3	Ia-Iab	-7.71
17656	SMC	00:50:47.16	-72:42:57.72	yes	B	4045	71	-0.89	0.08	K0	Ia-Iab	-7.51
17656	SMC	00:50:47.16	-72:42:57.72	yes	A	4101	201	-0.85	0.21	G8.5	Iab	-7.51
17656	SMC	00:50:47.16	-72:42:57.72	yes	C	4088	94	-0.82	0.10	K1	Ia-Iab	-7.51
18592	SMC	00:51:03.85	-72:43:17.88	yes	B	3960	67	-0.84	0.07	M1	Ia	-8.95
18592	SMC	00:51:03.85	-72:43:17.88	yes	A	3877	68	-0.92	0.07	M3	Ia-Iab	-8.95
18592	SMC	00:51:03.85	-72:43:17.88	yes	C	4011	71	-0.74	0.07	M0.5	Ia	-8.95
19551	SMC	00:51:20.18	-72:49:22.66	yes	B	3973	81	-0.90	0.08	K1	Iab-Ib	-6.96
19551	SMC	00:51:20.18	-72:49:22.66	yes	A	4010	229	-0.86	0.22	K0	Iab	-6.96
19551	SMC	00:51:20.18	-72:49:22.66	yes	C	4008	120	-0.89	0.11	K2	Iab-Ib	-6.96
19743	SMC	00:51:23.27	-72:38:44.19	yes	B	4108	83	-0.64	0.08	K2	Ia-Iab	-7.66
19743	SMC	00:51:23.27	-72:38:44.19	yes	A	3933	97	-0.77	0.09	M1	Ia-Iab	-7.66
19743	SMC	00:51:23.27	-72:38:44.19	yes	C	4065	86	-0.71	0.09	K3.5	Ia	-7.66
20133	SMC	00:51:29.67	-73:10:44.40	yes	B	3973	73	-0.60	0.06	K3	Iab-Ib	-8.08
20133	SMC	00:51:29.67	-73:10:44.40	yes	A	3897	147	-0.47	0.12	M1.5	Ia	-8.08
20133	SMC	00:51:29.67	-73:10:44.40	yes	C	4006	70	-0.52	0.06	K4	Ia	-8.08
20612	SMC	00:51:37.65	-72:25:59.56	yes	B	4061	112	-1.03	0.13	K0.5	Iab	-6.92
20612	SMC	00:51:37.65	-72:25:59.56	yes	A	4168	135	-0.87	0.15	G8	Iab	-6.92
20612	SMC	00:51:37.65	-72:25:59.56	yes	C	4205	183	-0.84	0.20	G8	Ia-Iab	-6.92
23463	SMC	00:52:26.49	-72:45:16.10	yes	B	3983	70	-0.72	0.07	K5	Iab	-7.66

Table A2: continued.

ID	Cloud	RA J2000	DEC J2000	Var.	Epochs	T_{eff} (K)	ΔT_{eff} (K)	[M/H] (dex)	Δ [M/H] (dex)	SpT	LC	M_{bol} (mag)
23463	SMC	00:52:26.49	-72:45:16.10	yes	A	3843	91	-0.71	0.08	M1	Ia-Iab	-7.66
23463	SMC	00:52:26.49	-72:45:16.10	yes	C	4162	92	-0.85	0.11	K0	Ia	-7.66
23700	SMC	00:52:30.74	-72:26:46.72	no	A, B, C	4018	61	-0.94	0.06	K0	Iab	-6.90
25550	SMC	00:53:02.91	-73:07:46.01	no	A, B, C	3980	67	-0.71	0.06	K3	Iab	-6.80
25879	SMC	00:53:08.96	-72:29:38.55	yes	B	4127	72	-0.63	0.07	K1	Ia-Iab	-7.99
25879	SMC	00:53:08.96	-72:29:38.55	yes	A	4096	64	-0.75	0.07	K4	Ia	-7.99
25879	SMC	00:53:08.96	-72:29:38.55	yes	C	4203	70	-0.58	0.07	K3	Ia	-7.99
25888	SMC	00:53:09.11	-73:04:03.98	yes	B	4017	62	-0.76	0.07	K2.5	Ia-Iab	-8.04
25888	SMC	00:53:09.11	-73:04:03.98	yes	A	4007	127	-0.70	0.12	K4	Ia-Iab	-8.04
25888	SMC	00:53:09.11	-73:04:03.98	yes	C	4039	64	-0.71	0.06	K4.5	Ia-Iab	-8.04
26402	SMC	00:53:17.73	-72:46:07.15	yes	B	3998	87	-0.81	0.09	K2.5	Ia-Iab	-7.04
26402	SMC	00:53:17.73	-72:46:07.15	yes	A	4068	92	-0.74	0.09	K3	Iab	-7.04
26402	SMC	00:53:17.73	-72:46:07.15	yes	C	4077	120	-0.83	0.13	K0	Ia-Iab	-7.04
26778	SMC	00:53:24.63	-73:18:31.60	yes	B	4060	79	-0.56	0.08	K2	Ia-Iab	-7.14
26778	SMC	00:53:24.63	-73:18:31.60	yes	A	4091	283	-0.61	0.26	G7	Iab	-7.14
26778	SMC	00:53:24.63	-73:18:31.60	yes	C	4196	114	-0.63	0.12	G8	Ia-Iab	-7.14
27443	SMC	00:53:36.42	-73:01:34.92	yes	B	3951	65	-0.74	0.06	K3	Iab-Ib	-7.69
27443	SMC	00:53:36.42	-73:01:34.92	yes	A	3922	127	-0.70	0.11	K4	Ia-Iab	-7.69
27443	SMC	00:53:36.42	-73:01:34.92	yes	C	4028	81	-0.77	0.08	K2	Iab	-7.69
27945	SMC	00:53:45.76	-72:53:38.86	yes	B	4309	122	-0.76	0.15	K0	Iab	-6.97
27945	SMC	00:53:45.76	-72:53:38.86	yes	A	4385	246	-0.67	0.31	G6	Iab	-6.97
27945	SMC	00:53:45.76	-72:53:38.86	yes	C	4367	141	-0.71	0.18	G5.5	Iab	-6.97
30135	SMC	00:54:26.86	-72:52:59.69	no	A, B, C	4325	72	-0.10	0.07	G7.5	Iab	-7.05
30616	SMC	00:54:35.89	-72:34:14.47	yes	B	4167	91	-0.70	0.10	K0	Ia-Iab	-8.02
30616	SMC	00:54:35.89	-72:34:14.47	yes	A	4120	79	-0.63	0.08	K2.5	Ia-Iab	-8.02
30616	SMC	00:54:35.89	-72:34:14.47	yes	C	4132	91	-0.68	0.09	K1	Ia-Iab	-8.02
32188	SMC	00:55:03.76	-73:00:36.75	yes	B	4318	91	-0.62	0.11	G6	Ia	-7.65
32188	SMC	00:55:03.76	-73:00:36.75	yes	A	4191	224	-0.70	0.24	G8	Ia-Iab	-7.65
32188	SMC	00:55:03.76	-73:00:36.75	yes	C	4298	100	-0.64	0.12	G6	Ia-Iab	-7.65
33610	SMC	00:55:26.74	-72:35:56.31	yes	B	4032	74	-0.82	0.08	K2	Iab	-7.50
33610	SMC	00:55:26.74	-72:35:56.31	yes	A	4057	59	-0.79	0.07	K5	Ia	-7.50
33610	SMC	00:55:26.74	-72:35:56.31	yes	C	4084	84	-0.68	0.08	K4	Ia-Iab	-7.50
34158	SMC	00:55:36.58	-72:36:24.11	yes	B	4090	81	-0.64	0.08	K1	Ia-Iab	-7.45
34158	SMC	00:55:36.58	-72:36:24.11	yes	A	4045	88	-0.65	0.08	K2.5	Ia-Iab	-7.45
34158	SMC	00:55:36.58	-72:36:24.11	yes	C	4119	85	-0.62	0.08	K3	Ia-Iab	-7.45
35231	SMC	00:55:55.07	-72:40:30.64	yes	B	4494	143	-0.92	0.20	G3.5	Ia	-7.53
35231	SMC	00:55:55.07	-72:40:30.64	yes	A	4658	130	-0.76	0.17	G1	Iab	-7.53
35231	SMC	00:55:55.07	-72:40:30.64	yes	C	4654	197	-0.77	0.26	G6	Ia	-7.53
37994	SMC	00:56:43.46	-72:30:15.11	no	A, B, C	3924	39	-0.88	0.04	K2.5	Iab	-7.51
41778	SMC	00:57:56.30	-72:17:33.81	no	A, B, C	4008	45	-0.81	0.05	K1.5	Iab	-7.31
42319	SMC	00:58:06.54	-72:21:00.22	no	A, B, C	3993	45	-0.79	0.04	K1.5	Iab-Ib	-7.13
42438	SMC	00:58:08.64	-72:19:27.19	yes	B	4003	88	-0.81	0.09	K0.5	Ib	-6.93
42438	SMC	00:58:08.64	-72:19:27.19	yes	A	4025	66	-0.82	0.07	K1.5	Iab-Ib	-6.93
42438	SMC	00:58:08.64	-72:19:27.19	yes	C	4039	103	-0.83	0.11	K2	Iab-Ib	-6.93
43219	SMC	00:58:23.33	-72:48:41.16	no	A, B, C	4009	57	-0.72	0.05	K3	Iab-Ib	-7.13
43725	SMC	00:58:33.13	-72:19:16.09	yes	B	3994	99	-0.92	0.10	K0	Iab-Ib	-6.71
43725	SMC	00:58:33.13	-72:19:16.09	yes	A	3968	67	-0.90	0.07	K1	Iab	-6.71
43725	SMC	00:58:33.13	-72:19:16.09	yes	C	4023	112	-0.80	0.11	K2	Ib	-6.71
45378	SMC	00:59:07.14	-72:13:08.82	no	A, B, C	4048	42	-0.75	0.04	K1	Iab	-7.27
45850	SMC	00:59:16.84	-72:25:11.23	yes	B	4050	93	-0.95	0.11	K2	Iab	-7.19
45850	SMC	00:59:16.84	-72:25:11.23	yes	A	4019	71	-0.91	0.07	K1	Iab	-7.19
45850	SMC	00:59:16.84	-72:25:11.23	yes	C	4111	115	-0.87	0.12	G7	Ia-Iab	-7.19
46497	SMC	00:59:31.33	-72:15:46.58	yes	B	3957	65	-0.71	0.06	K3	Iab	-7.86
46497	SMC	00:59:31.33	-72:15:46.58	yes	A	3940	52	-0.70	0.05	K5.5	Ia-Iab	-7.86
46497	SMC	00:59:31.33	-72:15:46.58	yes	C	3955	72	-0.66	0.06	K5	Iab	-7.86
46662	SMC	00:59:34.97	-72:04:06.67	yes	B	4016	64	-0.66	0.07	K3	Iab	-7.93

Table A2: continued.

ID	Cloud	RA J2000	DEC J2000	Var.	Epochs	T_{eff} (K)	ΔT_{eff} (K)	[M/H] (dex)	Δ [M/H] (dex)	SpT	LC	M_{bol} (mag)
46662	SMC	00:59:34.97	-72:04:06.67	yes	A	4029	55	-0.70	0.06	K1.5	Ia	-7.93
46662	SMC	00:59:34.97	-72:04:06.67	yes	C	3945	70	-0.60	0.05	M0.5	Iab	-7.93
46910	SMC	00:59:40.53	-72:20:55.93	no	A, B, C	4193	49	-0.79	0.06	G7.5	Ia-Iab	-7.13
47757	SMC	01:00:00.58	-72:19:40.15	yes	B	4091	73	-0.85	0.09	K1	Iab	-8.01
47757	SMC	01:00:00.58	-72:19:40.15	yes	A	4094	57	-0.80	0.06	K0.5	Ia	-8.01
47757	SMC	01:00:00.58	-72:19:40.15	yes	C	4164	82	-0.72	0.08	G8	Iab	-8.01
48122	SMC	01:00:09.35	-72:08:44.24	yes	B	4081	80	-0.79	0.09	K0	Iab	-7.40
48122	SMC	01:00:09.35	-72:08:44.24	yes	A	4055	64	-0.76	0.07	K1.5	Iab	-7.40
48122	SMC	01:00:09.35	-72:08:44.24	yes	C	4071	97	-0.77	0.10	K0	Iab	-7.40
49033	SMC	01:00:30.52	-71:58:24.45	yes	B	4089	102	-0.83	0.13	K1	Iab	-7.59
49033	SMC	01:00:30.52	-71:58:24.45	yes	A	4114	65	-0.78	0.08	G7.5	Ia-Iab	-7.59
49033	SMC	01:00:30.52	-71:58:24.45	yes	C	4130	89	-0.73	0.09	G8	Iab	-7.59
49428	SMC	01:00:40.29	-72:35:59.36	yes	B	4165	116	-0.69	0.12	K1	Iab	-7.09
49428	SMC	01:00:40.29	-72:35:59.36	yes	A	4127	81	-0.80	0.09	G7.5	Iab	-7.09
49428	SMC	01:00:40.29	-72:35:59.36	yes	C	4131	110	-0.89	0.12	G7	Iab	-7.09
49478	SMC	01:00:41.52	-72:10:37.07	yes	B	3974	67	-0.56	0.06	K5	Ia-Iab	-8.37
49478	SMC	01:00:41.52	-72:10:37.07	yes	A	4017	60	-0.75	0.07	M0	Ia	-8.37
49478	SMC	01:00:41.52	-72:10:37.07	yes	C	4170	74	-0.54	0.07	K4	Ia-Iab	-8.37
49990	SMC	01:00:54.15	-72:51:36.66	yes	B	4258	89	-0.38	0.09	K1	Ia-Iab	-7.87
49990	SMC	01:00:54.15	-72:51:36.66	yes	A	4404	86	-0.41	0.11	G5.5	Ia	-7.87
49990	SMC	01:00:54.15	-72:51:36.66	yes	C	4477	57	-0.47	0.08	G4	Ia	-7.87
50237	SMC	01:01:00.32	-72:13:42.00	yes	B	4152	116	-0.86	0.13	K0	Iab	-6.92
50237	SMC	01:01:00.32	-72:13:42.00	yes	A	4162	71	-0.83	0.08	G7.5	Iab	-6.92
50237	SMC	01:01:00.32	-72:13:42.00	yes	C	4189	114	-0.84	0.13	G7	Ia	-6.92
50348	SMC	01:01:03.30	-72:04:39.46	no	A, B, C	4126	59	-0.79	0.07	K0	Iab	-7.06
50360	SMC	01:01:03.65	-72:02:58.75	no	A, B, C	3963	57	-1.00	0.06	K1.5	Iab-Ib	-6.88
50840	SMC	01:01:15.96	-72:13:10.35	yes	B	3937	62	-0.69	0.05	K3	Iab	-7.93
50840	SMC	01:01:15.96	-72:13:10.35	yes	A	3867	54	-0.81	0.05	M0	Ia-Iab	-7.93
50840	SMC	01:01:15.96	-72:13:10.35	yes	C	3916	64	-0.64	0.05	M0	Ia-Iab	-7.93
51000	SMC	01:01:19.93	-72:05:13.44	yes	B	4130	124	-0.71	0.13	K1	Iab	-7.10
51000	SMC	01:01:19.93	-72:05:13.44	yes	A	4125	72	-0.77	0.08	K0	Iab	-7.10
51000	SMC	01:01:19.93	-72:05:13.44	yes	C	4141	101	-0.66	0.10	G7	Iab	-7.10
51265	SMC	01:01:26.91	-72:01:41.38	yes	B	4060	137	-0.88	0.15	K2	Iab	-7.09
51265	SMC	01:01:26.91	-72:01:41.38	yes	A	4045	75	-0.98	0.09	K0.5	Iab	-7.09
51265	SMC	01:01:26.91	-72:01:41.38	yes	C	4131	101	-0.83	0.11	K1	Iab	-7.09
51906	SMC	01:01:43.59	-72:38:25.45	yes	B	4013	103	-0.99	0.12	K2	Iab	-6.95
51906	SMC	01:01:43.59	-72:38:25.45	yes	A	4012	100	-0.96	0.11	K0.5	Iab	-6.95
51906	SMC	01:01:43.59	-72:38:25.45	yes	C	4038	113	-0.99	0.12	K0	Iab-Ib	-6.95
52334	SMC	01:01:54.20	-71:52:18.63	yes	B	3860	169	-0.78	0.16	K3	Iab	-7.63
52334	SMC	01:01:54.20	-71:52:18.63	yes	A	3934	60	-0.76	0.06	K4	Ia-Iab	-7.63
52334	SMC	01:01:54.20	-71:52:18.63	yes	C	3896	92	-0.54	0.07	M0	Iab	-7.63
52389	SMC	01:01:55.48	-72:00:29.36	no	A, B, C	3957	47	-0.79	0.05	K3.5	Iab	-7.41
53557	SMC	01:02:23.80	-72:55:21.22	yes	B	4066	106	-0.86	0.12	K2	Ia-Iab	-7.32
53557	SMC	01:02:23.80	-72:55:21.22	yes	A	4014	107	-0.88	0.11	K0.5	Iab-Ib	-7.32
53557	SMC	01:02:23.80	-72:55:21.22	yes	C	4050	79	-0.89	0.09	K1.5	Iab	-7.32
53638	SMC	01:02:25.80	-72:38:57.18	no	A, B, C	3962	50	-0.88	0.05	K1	Iab	-6.91
54111	SMC	01:02:37.27	-72:16:25.09	yes	B	4136	113	-0.95	0.13	G8	Ia-Iab	-7.49
54111	SMC	01:02:37.27	-72:16:25.09	yes	A	4213	73	-0.86	0.09	G6	Ia-Iab	-7.49
54111	SMC	01:02:37.27	-72:16:25.09	yes	C	4147	131	-0.86	0.13	G7.5	Iab	-7.49
54300	SMC	01:02:42.07	-72:37:29.29	yes	B	3997	90	-0.94	0.10	K1.5	Iab	-7.07
54300	SMC	01:02:42.07	-72:37:29.29	yes	A	4017	73	-0.94	0.08	K0.5	Iab	-7.07
54300	SMC	01:02:42.07	-72:37:29.29	yes	C	4040	105	-0.97	0.11	K2	Iab-Ib	-7.07
54414	SMC	01:02:44.80	-72:01:51.70	yes	B	4122	212	-0.82	0.23	K0	Iab	-6.99
54414	SMC	01:02:44.80	-72:01:51.70	yes	A	4084	76	-0.86	0.08	K0.5	Ia-Iab	-6.99
54414	SMC	01:02:44.80	-72:01:51.70	yes	C	4130	109	-0.78	0.12	G8	Iab-Ib	-6.99
54708	SMC	01:02:51.46	-72:24:15.42	yes	B	4147	90	-0.86	0.11	K1	Ia-Iab	-7.27

Table A2: continued.

ID	Cloud	RA J2000	DEC J2000	Var.	Epochs	T_{eff} (K)	ΔT_{eff} (K)	[M/H] (dex)	Δ [M/H] (dex)	SpT	LC	M_{bol} (mag)
54708	SMC	01:02:51.46	-72:24:15.42	yes	A	4165	74	-0.83	0.09	G8	Ia-Iab	-7.27
54708	SMC	01:02:51.46	-72:24:15.42	yes	C	4125	96	-0.85	0.11	G7.5	Iab	-7.27
55188	SMC	01:03:02.45	-72:01:52.99	yes	B	4248	194	-0.72	0.24	K4.5	Ia-Iab	-7.38
55188	SMC	01:03:02.45	-72:01:52.99	yes	A	3916	62	-0.81	0.06	M1.5	Ia	-7.38
55275	SMC	01:03:04.30	-72:34:12.99	yes	B	3908	70	-0.76	0.07	K3.5	Iab	-7.56
55275	SMC	01:03:04.30	-72:34:12.99	yes	A	3916	60	-0.82	0.06	K2.5	Ia-Iab	-7.56
55275	SMC	01:03:04.30	-72:34:12.99	yes	C	3915	70	-0.76	0.06	K5	Iab	-7.56
55355	SMC	01:03:06.47	-72:28:35.46	yes	B	4141	92	-0.79	0.11	K2	Ia-Iab	-7.48
55355	SMC	01:03:06.47	-72:28:35.46	yes	A	3955	67	-0.77	0.06	K4	Ia-Iab	-7.48
55355	SMC	01:03:06.47	-72:28:35.46	yes	C	4167	98	-0.66	0.10	K1	Ia	-7.48
55470	SMC	01:03:08.94	-71:55:50.86	yes	B	4142	407	-0.80	0.44	K0	Iab	-6.94
55470	SMC	01:03:08.94	-71:55:50.86	yes	A	4188	95	-0.77	0.11	G7.5	Iab	-6.94
55470	SMC	01:03:08.94	-71:55:50.86	yes	C	4152	136	-0.72	0.14	K2	Ia-Iab	-6.94
55560	SMC	01:03:10.93	-72:18:32.81	yes	B	3978	78	-0.75	0.08	K3	Iab-Ib	-7.09
55560	SMC	01:03:10.93	-72:18:32.81	yes	A	3999	62	-0.79	0.06	K1	Ia-Iab	-7.09
55560	SMC	01:03:10.93	-72:18:32.81	yes	C	4054	87	-0.72	0.08	K1	Ia-Iab	-7.09
55681	SMC	01:03:12.97	-72:09:26.32	yes	B	3941	88	-0.85	0.09	K5	Iab	-7.66
55681	SMC	01:03:12.97	-72:09:26.32	yes	A	4007	53	-0.72	0.06	K4	Ia	-7.66
55681	SMC	01:03:12.97	-72:09:26.32	yes	C	3904	69	-0.78	0.06	M1.5	Ia	-7.66
55933	SMC	01:03:18.56	-72:06:46.19	yes	A	4069	82	-0.91	0.09	K1	Ia-Iab	-7.25
55933	SMC	01:03:18.56	-72:06:46.19	yes	C	4035	89	-0.73	0.09	K4	Ia-Iab	-7.25
56389	SMC	01:03:27.61	-72:52:09.76	yes	B	4053	84	-0.59	0.08	K3.5	Ia-Iab	-8.51
56389	SMC	01:03:27.61	-72:52:09.76	yes	A	4099	77	-0.51	0.07	K3	Iab	-8.51
56389	SMC	01:03:27.61	-72:52:09.76	yes	C	4002	90	-0.61	0.07	K5	Iab	-8.51
56732	SMC	01:03:34.42	-72:06:06.75	yes	B	3844	118	-0.84	0.11	M0	Iab-Ib	-7.36
56732	SMC	01:03:34.42	-72:06:06.75	yes	A	3862	70	-0.85	0.07	K4	Iab-Ib	-7.36
56732	SMC	01:03:34.42	-72:06:06.75	yes	C	3939	84	-0.76	0.08	K3.5	Iab	-7.36
57386	SMC	01:03:47.35	-72:01:15.92	yes	B	3992	150	-0.91	0.16	M0.5	Iab	-7.31
57386	SMC	01:03:47.35	-72:01:15.92	yes	A	4049	74	-0.89	0.08	K2	Iab	-7.31
57472	SMC	01:03:49.01	-72:02:12.83	no	A, B, C	4042	56	-0.77	0.06	K1.5	Iab	-7.30
58149	SMC	01:04:02.77	-72:05:27.72	no	A, B, C	4034	52	-0.79	0.05	K0.5	Iab-Ib	-7.07
58472	SMC	01:04:09.51	-72:50:15.94	yes	B	4125	130	-0.68	0.14	K3	Ia-Iab	-7.01
58472	SMC	01:04:09.51	-72:50:15.94	yes	A	4095	75	-0.73	0.08	K0.5	Iab	-7.01
58472	SMC	01:04:09.51	-72:50:15.94	yes	C	4126	105	-0.69	0.11	K3	Iab	-7.01
58738	SMC	01:04:15.49	-72:45:20.16	yes	B	4688	193	-0.20	0.24	G7	Ia	-7.13
58839	SMC	01:04:17.70	-71:57:32.59	yes	B	4139	289	-0.75	0.28	K2	Ib	-6.92
58839	SMC	01:04:17.70	-71:57:32.59	yes	A	4069	72	-0.85	0.08	G8.5	Ia-Iab	-6.92
58839	SMC	01:04:17.70	-71:57:32.59	yes	C	4136	131	-0.73	0.13	G7.5	Iab	-6.92
59426	SMC	01:04:30.28	-72:04:36.17	yes	B	3859	157	-0.73	0.14	K1.5	Ib	-7.30
59426	SMC	01:04:30.28	-72:04:36.17	yes	A	3907	59	-0.84	0.06	K3	Iab-Ib	-7.30
59426	SMC	01:04:30.28	-72:04:36.17	yes	C	3894	90	-0.64	0.07	K4	Iab	-7.30
59803	SMC	01:04:38.21	-72:01:27.01	yes	B	4092	112	-0.70	0.12	K0.5	Ia-Iab	-8.23
59803	SMC	01:04:38.21	-72:01:27.01	yes	A	4203	69	-0.61	0.07	G7	Ia	-8.23
59803	SMC	01:04:38.21	-72:01:27.01	yes	C	4192	85	-0.49	0.08	K3	Ia-Iab	-8.23
60447	SMC	01:04:53.10	-72:47:49.16	yes	B	3966	295	-0.59	0.24	K2	Ia-Iab	-7.03
60447	SMC	01:04:53.10	-72:47:49.16	yes	A	3890	79	-0.79	0.07	K4	Iab	-7.03
60447	SMC	01:04:53.10	-72:47:49.16	yes	C	4009	87	-0.75	0.09	K1.5	Ia-Iab	-7.03
61296	SMC	01:05:11.60	-72:02:27.57	yes	B	4311	423	-0.72	0.52	G6	Iab	-7.14
61296	SMC	01:05:11.60	-72:02:27.57	yes	A	4124	72	-0.84	0.09	G8	Ia-Iab	-7.14
61296	SMC	01:05:11.60	-72:02:27.57	yes	C	4166	127	-0.67	0.13	K2	Iab	-7.14
62427	SMC	01:05:40.05	-71:58:46.44	yes	A	4066	77	-0.81	0.08	G7.5	Ia-Iab	-6.94
62427	SMC	01:05:40.05	-71:58:46.44	yes	C	4207	174	-0.73	0.18	K0.5	Iab	-6.94
63114	SMC	01:06:01.35	-72:52:43.38	yes	A	3941	62	-0.63	0.05	M0	Iab	-7.51
63114	SMC	01:06:01.35	-72:52:43.38	yes	C	4150	98	-0.67	0.09	K1	Iab	-7.51
63131	SMC	01:06:01.71	-72:24:03.74	yes	B	4014	172	-0.96	0.18	K0	Iab-Ib	-6.83
63131	SMC	01:06:01.71	-72:24:03.74	yes	A	4151	79	-0.83	0.09	G7	Iab	-6.83

Table A2: continued.

ID	Cloud	RA J2000	DEC J2000	Var.	Epochs	T_{eff} (K)	ΔT_{eff} (K)	[M/H] (dex)	$\Delta[M/H]$ (dex)	SpT	LC	M_{bol} (mag)
63131	SMC	01:06:01.71	-72:24:03.74	yes	C	4167	102	-0.86	0.12	G8	Iab	-6.83
63188	SMC	01:06:03.20	-72:52:16.51	no	B	3914	339	-0.63	0.24	K4	Iab-Ib	-7.11
64448	SMC	01:06:40.19	-72:28:45.26	no	A, B, C	4360	68	-0.74	0.09	G5	Ia-Iab	-6.99
64663	SMC	01:06:47.66	-72:16:11.63	yes	B	4044	120	-0.75	0.13	K3	Ia-Iab	-8.10
64663	SMC	01:06:47.66	-72:16:11.63	yes	A	4117	73	-0.73	0.08	K3.5	Ia-Iab	-8.10
64663	SMC	01:06:47.66	-72:16:11.63	yes	C	4207	80	-0.53	0.08	G6	Ia	-8.10
66066	SMC	01:07:29.48	-72:30:45.68	yes	B	4128	267	-0.85	0.29	K0.5	Iab	-7.30
66066	SMC	01:07:29.48	-72:30:45.68	yes	A	4104	88	-0.87	0.10	G7.5	Iab	-7.30
66066	SMC	01:07:29.48	-72:30:45.68	yes	C	4154	99	-0.78	0.10	G6.5	Ia-Iab	-7.30
66694	SMC	01:07:48.92	-72:23:42.37	yes	B	3943	146	-0.89	0.15	K2	Ia-Iab	-7.52
66694	SMC	01:07:48.92	-72:23:42.37	yes	A	4027	76	-0.91	0.08	K0.5	Iab	-7.52
66694	SMC	01:07:48.92	-72:23:42.37	yes	C	4034	75	-0.84	0.08	K1.5	Ia-Iab	-7.52
67554	SMC	01:08:14.79	-72:46:40.99	yes	A	4059	82	-0.76	0.09	K2	Iab	-7.21
67554	SMC	01:08:14.79	-72:46:40.99	yes	C	4133	105	-0.69	0.10	G8	Ia-Iab	-7.21
68648	SMC	01:08:52.06	-72:23:07.38	no	A, C	4111	55	-0.89	0.06	G7.5	Iab	-7.65
71566	SMC	01:10:53.49	-72:25:40.12	no	C	4110	119	-0.74	0.12	K0	Ia-Iab	-6.96
105-11	SMC	00:53:47.92	-72:02:09.45	yes	B	3961	83	-0.68	0.07	K3.5	Ia-Iab	-8.04
105-11	SMC	00:53:47.92	-72:02:09.45	yes	A	3854	76	-0.48	0.06	M1.5	Ia-Iab	-8.04
105-11	SMC	00:53:47.92	-72:02:09.45	yes	C	4060	78	-0.54	0.07	K3	Ia	-8.04
105-21	SMC	00:55:22.35	-72:16:38.52	yes	B	4174	182	-1.05	0.22	K0	Iab-Ib	-6.29
105-21	SMC	00:55:22.35	-72:16:38.52	yes	A	4157	138	-1.03	0.16	G7.5	Iab	-6.29
105-21	SMC	00:55:22.35	-72:16:38.52	yes	C	4242	240	-0.90	0.27	G7	Iab	-6.29
106-5	SMC	00:51:50.50	-72:11:32.72	yes	B	4035	100	-0.93	0.12	K0	Iab	-7.36
106-5	SMC	00:51:50.50	-72:11:32.72	yes	A	4024	59	-0.87	0.07	K1	Ia-Iab	-7.36
106-5	SMC	00:51:50.50	-72:11:32.72	yes	C	4096	127	-0.75	0.12	K3	Ia-Iab	-7.36
106-9	SMC	00:52:31.48	-72:11:37.58	yes	B	4172	138	-0.86	0.15	K0	Ia-Iab	-7.06
106-9	SMC	00:52:31.48	-72:11:37.58	yes	A	4170	78	-0.77	0.09	G6.5	Ia-Iab	-7.06
106-9	SMC	00:52:31.48	-72:11:37.58	yes	C	4240	142	-0.77	0.16	G8	Iab	-7.06
108-8	SMC	00:54:54.39	-73:09:03.44	no	A, B, C	4503	124	-0.69	0.16	G5.5	Ia-Iab	-6.50
114-3	SMC	00:55:58.79	-73:20:41.32	yes	B	4074	98	-0.83	0.12	K0	Iab-Ib	-7.34
114-3	SMC	00:55:58.79	-73:20:41.32	yes	C	4025	84	-0.74	0.08	K3	Iab-Ib	-7.34
116-15	SMC	01:02:39.91	-72:11:27.22	yes	C	4374	277	-0.96	0.38	G6	Iab-Ib	-6.44
SkKM13	SMC	00:45:04.57	-73:05:27.56	yes	B	3841	70	-0.66	0.06	M1	Ia-Iab	-8.08
SkKM13	SMC	00:45:04.57	-73:05:27.56	yes	A	3684	298	-0.53	0.27	M3	Ia	-8.08
SkKM13	SMC	00:45:04.57	-73:05:27.56	yes	C	3832	102	-0.38	0.07	M1.5	Ia	-8.08
SkKM63	SMC	00:50:56.04	-72:15:06.02	yes	B	3990	63	-0.49	0.06	K3	Ia-Iab	-8.40
SkKM63	SMC	00:50:56.04	-72:15:06.02	yes	A	4020	58	-0.66	0.06	K5	Ia-Iab	-8.40
SkKM63	SMC	00:50:56.04	-72:15:06.02	yes	C	4027	73	-0.50	0.06	K5	Ia-Iab	-8.40
SkKM78	SMC	00:51:50.26	-72:05:57.58	no	A, B, C	3980	46	-0.71	0.04	K3.5	Iab	-7.44
SkKM89	SMC	00:52:25.33	-72:25:13.37	no	A, B	4111	72	-0.90	0.08	G8.5	Iab	-6.99
SkKM89b	SMC	00:52:34.22	-72:24:52.30	no	A, B	3781	63	-1.01	0.07	K4	Ib	-6.39
SMC 019	SMC	00:36:09.20	-73:43:14.94	no	C	3828	152	-0.86	0.14	K3	Ib	-5.98
SMC 024	SMC	00:36:47.53	-73:20:43.32	no	C	4008	121	-0.75	0.11	K2	Iab-Ib	-6.85
SMC 027	SMC	00:37:59.51	-73:27:39.27	no	C	4506	355	-0.50	0.41	G7	Iab	-5.70
SMC 028	SMC	00:38:06.24	-73:46:48.19	no	C	4216	153	-0.88	0.17	G7	Iab	-7.02
SMC 030	SMC	00:38:17.31	-73:54:01.27	no	C	3799	244	-0.98	0.22	K4	Ib	-5.53
SMC 051	SMC	00:42:04.58	-72:34:10.68	no	C	4139	149	-0.68	0.14	K1	Iab	-7.02
SMC 055	SMC	00:42:23.63	-73:24:43.54	no	C	4887	451	-0.31	0.42	G8	Iab	-5.66
SMC 065	SMC	00:43:46.11	-73:28:40.46	no	C	3925	156	-0.96	0.14	K2	Iab-Ib	-6.50
SMC 066	SMC	00:43:58.63	-73:28:47.52	no	C	4667	582	-0.66	0.70	K0	Iab-Ib	-5.60
SMC 079	SMC	00:45:03.16	-72:55:15.62	no	C	4172	233	-0.81	0.26	G8	Ib	-6.09
SMC 085	SMC	00:45:35.78	-73:17:37.24	no	C	4475	433	-0.55	0.51	K0	Ib	-5.67
SMC 086	SMC	00:45:36.78	-73:08:45.23	no	C	4124	189	-0.59	0.17	K2	Ia-Iab	-6.53
SMC 091	SMC	00:46:16.61	-72:40:35.45	no	C	4041	173	-0.54	0.14	K4	Ia	-7.21
SMC 092	SMC	00:46:19.64	-73:19:31.42	no	C	3992	150	-0.71	0.13	K3	Iab	-6.64
SMC 096	SMC	00:46:33.28	-73:26:18.35	no	C	4556	489	-0.18	0.51	K3	Ib	-5.49
SMC 099	SMC	00:46:41.68	-73:22:54.20	no	C	5309	568	-0.09	0.33	G7	Ia-Iab	-5.64

Table A2: continued.

ID	Cloud	RA J2000	DEC J2000	Var.	Epochs	T_{eff} (K)	ΔT_{eff} (K)	[M/H] (dex)	Δ [M/H] (dex)	SpT	LC	M_{bol} (mag)
SMC 103	SMC	00:46:48.79	-73:33:48.38	no	C	5450	314	-1.06	0.23	G5	Ib	-6.97
SMC 106	SMC	00:46:56.38	-73:22:54.03	no	C	4169	192	-0.67	0.19	K1	Ia-Iab	-6.64
SMC 108	SMC	00:47:00.84	-73:23:25.48	no	C	3610	156	-0.71	0.15	M3	Iab	-6.60
SMC 109	SMC	00:47:01.82	-73:03:20.88	no	C	3787	181	-0.66	0.14	M1	Iab-Ib	-6.03
SMC 112	SMC	00:47:07.68	-73:44:43.41	no	C	4184	269	-0.86	0.29	G8	Ib	-6.00
SMC 114	SMC	00:47:12.94	-73:09:42.85	no	C	4189	327	-0.71	0.32	G8	Iab	-6.73
SMC 115	SMC	00:47:19.80	-73:10:40.75	no	C	4034	212	-0.76	0.20	K3	Iab	-7.03
SMC 121	SMC	00:47:53.48	-73:17:24.28	no	C	4607	516	-0.50	0.59	G8	Ib	-5.65
SMC 123	SMC	00:48:00.60	-73:17:21.39	no	C	4082	435	-0.80	0.34	K1	Iab	81.60
SMC 124	SMC	00:48:01.16	-73:23:13.42	no	C	4387	414	-0.62	0.49	G7	Ib	-5.53
SMC 126	SMC	00:48:02.28	-73:24:14.18	no	C	4439	476	-0.61	0.53	G8	Iab	-5.51
SMC 128	SMC	00:48:04.27	-72:52:42.11	no	C	4253	264	-0.79	0.30	G7.5	Iab	-6.28
SMC 130	SMC	00:48:13.02	-73:05:40.19	no	C	4127	291	-0.74	0.25	K1	Iab-Ib	-5.80
SMC 132	SMC	00:48:17.27	-73:51:25.37	no	C	4108	103	-0.46	0.09	K2	Ia-Iab	-7.32
SMC 135	SMC	00:48:27.64	-72:27:17.32	no	C	3944	97	-0.77	0.09	K4.5	Iab	-7.33
SMC 137	SMC	00:48:33.29	-73:12:33.33	no	C	4494	435	-0.67	0.58	G5	Ia-Iab	-5.46
SMC 138	SMC	00:48:37.45	-73:13:06.35	no	C	4073	155	-0.81	0.15	K1	Iab	-6.57
SMC 142	SMC	00:48:49.97	-73:20:03.47	no	C	4021	226	-0.63	0.18	K2	Ia-Iab	-6.81
SMC 144	SMC	00:49:03.66	-73:26:25.08	no	C	4151	139	-0.66	0.13	K1	Iab	-6.77
SMC 151	SMC	00:49:26.47	-73:04:35.51	no	C	4305	174	-0.69	0.20	G6.5	Ia-Iab	-6.50
SMC 160	SMC	00:49:51.21	-73:19:59.49	no	C	3947	229	-0.83	0.18	K1.5	Iab	-6.44
SMC 163	SMC	00:49:56.99	-73:28:25.60	no	C	4304	223	-0.63	0.24	G7	Iab	-5.76
SMC 164	SMC	00:49:57.37	-73:37:39.86	no	C	3933	105	-0.84	0.09	K4	Ia-Iab	-7.32
SMC 168	SMC	00:50:13.38	-73:02:37.87	no	C	4187	516	-0.88	0.54	K0	Iab-Ib	-5.47
SMC 171	SMC	00:50:38.38	-73:19:36.17	no	C	4107	281	-0.89	0.27	K2	Ib	-6.16
SMC 172	SMC	00:50:41.36	-73:11:51.97	no	C	4171	183	-0.77	0.18	G7.5	Ia-Iab	-6.29
SMC 176	SMC	00:50:48.01	-73:04:17.77	no	C	4044	300	-0.74	0.25	K1	Iab	-6.55
SMC 177	SMC	00:50:49.33	-73:15:46.64	no	C	4225	204	-0.66	0.21	K0.5	Iab	-6.40
SMC 178	SMC	00:50:50.49	-72:39:27.86	no	C	4104	280	-1.06	0.32	G8	Iab-Ib	-6.51
SMC 179	SMC	00:50:52.05	-73:28:51.75	no	C	4067	151	-0.70	0.14	K0.5	Iab	-6.65
SMC 180	SMC	00:50:58.02	-73:17:08.60	no	C	4284	483	-0.80	0.60	G8	Iab-Ib	-5.48
SMC 183	SMC	00:51:06.75	-73:16:36.76	no	C	4509	808	-0.59	0.86	K1	Iab-Ib	-6.02
SMC 184	SMC	00:51:10.66	-72:36:37.68	no	C	4517	603	-0.53	0.67	G7.5	Iab-Ib	-6.41
SMC 185	SMC	00:51:13.66	-73:32:40.92	no	C	3848	179	-0.61	0.14	K3.5	Ia-Iab	-6.20
SMC 187	SMC	00:51:17.87	-73:10:51.02	no	C	4226	380	-0.92	0.47	G7	Ib	-5.65
SMC 191	SMC	00:51:21.84	-73:08:21.09	no	C	3808	201	-0.90	0.18	K3	Ib-II	-5.78
SMC 194	SMC	00:51:26.53	-73:19:42.13	no	C	4097	190	-0.75	0.18	K1	Ia-Iab	-6.12
SMC 197	SMC	00:51:31.47	-73:10:51.41	no	C	4099	297	-0.71	0.23	K0	Iab	-6.47
SMC 198	SMC	00:51:32.80	-72:05:49.34	no	C	4077	121	-0.82	0.12	K0.5	Iab	-6.96
SMC 199	SMC	00:51:34.45	-72:49:56.77	no	C	3915	191	-0.61	0.14	K3	Iab-Ib	-6.14
SMC 202	SMC	00:51:38.78	-72:58:20.43	no	C	4322	392	-0.81	0.48	G7	Iab	-5.53
SMC 205	SMC	00:51:50.13	-72:37:27.64	no	C	4210	172	-0.82	0.19	G6.5	Iab	-6.75
SMC 206	SMC	00:51:50.49	-71:59:24.16	no	C	3912	100	-0.76	0.09	K3.5	Iab	-6.89
SMC 207	SMC	00:51:55.20	-73:14:38.82	no	C	4292	467	-0.83	0.60	K0	Ib	-5.51
SMC 209	SMC	00:52:02.77	-72:58:23.46	no	C	4049	156	-0.80	0.14	K1	Iab	-6.40
SMC 211	SMC	00:52:05.42	-72:43:13.24	no	C	3995	128	-0.91	0.12	K0.5	Iab	-6.83
SMC 214	SMC	00:52:12.05	-72:37:38.76	no	C	4782	412	-0.43	0.45	G5	Iab	-5.80
SMC 215	SMC	00:52:12.44	-73:24:55.95	no	C	4325	439	-0.83	0.54	G8.5	Ib	-5.49
SMC 217	SMC	00:52:14.02	-73:03:15.56	no	C	4056	388	-0.92	0.35	K2	Ib-II	-5.36
SMC 221	SMC	00:52:28.23	-73:19:15.90	no	C	4048	144	-0.70	0.13	G7.5	Iab	-6.87
SMC 224	SMC	00:52:38.26	-72:21:18.12	no	C	4131	101	-0.64	0.10	K2	Iab	-7.16
SMC 226	SMC	00:52:40.78	-73:18:34.97	no	C	4193	479	-0.80	0.50	G8	Iab	-6.51
SMC 227	SMC	00:52:41.42	-72:56:04.97	no	C	3645	327	-0.71	0.23	M2.5	Ia	-5.37
SMC 233	SMC	00:52:58.07	-72:36:31.74	no	C	3697	192	-0.84	0.19	M1	Iab-Ib	-6.07
SMC 235	SMC	00:52:59.07	-72:44:37.59	no	C	3812	265	-0.79	0.22	K3	Iab-Ib	-5.52
SMC 236	SMC	00:52:59.77	-73:26:31.07	no	C	4434	337	-0.74	0.44	G6	Iab	-5.81
SMC 242	SMC	00:53:16.80	-72:41:52.22	no	C	4196	554	-0.79	0.54	K2	Ib	-5.54

Table A2: continued.

ID	Cloud	RA J2000	DEC J2000	Var.	Epochs	T_{eff} (K)	ΔT_{eff} (K)	[M/H] (dex)	$\Delta[M/H]$ (dex)	SpT	LC	M_{bol} (mag)
SMC 244	SMC	00:53:18.60	-72:42:07.43	no	C	4035	179	-1.00	0.18	K0.5	Iab-Ib	-6.67
SMC 246	SMC	00:53:22.87	-72:11:47.19	no	C	4171	341	-0.96	0.39	G8	Ia-Iab	-6.53
SMC 248	SMC	00:53:24.67	-72:11:48.70	no	C	3988	135	-0.94	0.12	K0	Iab-Ib	-6.86
SMC 251	SMC	00:53:39.66	-72:32:08.87	no	C	4348	210	-0.82	0.26	G7.5	Ia-Iab	-6.75
SMC 252	SMC	00:53:41.55	-72:15:27.08	no	C	4127	134	-0.82	0.13	K2.5	Iab	-6.79
SMC 253	SMC	00:53:55.37	-72:06:43.28	no	C	4111	154	-0.86	0.15	K0	Iab	-6.71
SMC 260	SMC	00:54:30.01	-73:04:21.56	no	C	3751	288	-0.78	0.21	K3	Iab	-5.30
SMC 261	SMC	00:54:31.82	-73:17:03.84	no	C	4158	166	-0.74	0.16	K0	Iab	-6.70
SMC 263	SMC	00:54:40.40	-73:13:40.71	no	C	3739	200	-0.79	0.18	M0	Ib	-5.51
SMC 272	SMC	00:55:10.34	-74:01:49.45	no	C	3948	263	-0.85	0.21	K2	Ia-Iab	-5.80
SMC 273	SMC	00:55:17.12	-71:56:50.21	no	C	4148	93	-0.64	0.09	G7.5	Ia-Iab	-7.19
SMC 279	SMC	00:55:38.29	-73:18:25.14	no	C	4186	126	-0.80	0.14	G7	Iab-Ib	-6.56
SMC 280	SMC	00:55:38.46	-72:18:37.39	no	C	4158	110	-0.69	0.11	G7.5	Ia-Iab	-6.68
SMC 281	SMC	00:55:39.16	-73:08:50.61	no	C	4039	176	-0.95	0.16	K1	Ib	-6.15
SMC 286	SMC	00:56:18.24	-72:38:39.63	no	C	4124	146	-0.79	0.14	K0.5	Iab	-6.49
SMC 287	SMC	00:56:19.06	-72:28:08.27	no	C	4142	156	-0.87	0.16	G8.5	Iab-Ib	-6.42
SMC 294	SMC	00:57:06.79	-72:16:00.59	no	C	4092	122	-0.88	0.12	G8	Iab	-6.60
SMC 304	SMC	00:58:05.23	-72:17:25.87	no	C	4251	339	-0.87	0.41	G8	Iab	-6.55
SMC 306	SMC	00:58:24.81	-72:14:12.70	no	C	4090	151	-0.86	0.15	G8.5	Iab-Ib	-6.41
SMC 307	SMC	00:58:32.41	-72:33:28.27	no	C	4057	133	-0.76	0.12	K1	Iab	-6.62
SMC 312	SMC	00:58:50.91	-72:41:20.46	no	C	3914	132	-0.96	0.13	K1	Iab-Ib	-6.37
SMC 313	SMC	00:58:53.32	-72:08:35.40	no	C	4164	135	-0.91	0.14	G8	Iab-Ib	-6.82
SMC 320	SMC	01:00:03.49	-71:57:40.91	no	C	4198	152	-0.85	0.17	G8.5	Iab-Ib	-6.54
SMC 323	SMC	01:00:32.36	-72:08:50.97	no	C	4079	133	-0.79	0.12	K0	Ib	-6.41
SMC 324	SMC	01:00:44.44	-71:59:38.96	no	C	4084	143	-0.94	0.15	K1	Iab	-6.46
SMC 326	SMC	01:01:19.45	-72:06:48.53	no	C	4127	251	-0.85	0.26	K1	Iab	-6.77
SMC 330	SMC	01:01:44.01	-73:31:47.58	no	C	3791	156	-0.88	0.14	K4	Ib	-6.35
SMC 331	SMC	01:01:48.25	-72:40:50.66	no	C	3934	103	-0.83	0.09	K3	Iab-Ib	-6.61
SMC 332	SMC	01:01:52.87	-72:25:44.40	no	C	4060	149	-1.17	0.17	K1	Iab-Ib	-6.36
SMC 334	SMC	01:02:18.91	-72:02:34.08	no	C	4346	737	-0.50	0.67	G8.5	Iab	-6.76
SMC 339	SMC	01:02:34.43	-72:02:57.98	no	C	4229	345	-0.80	0.37	G8.5	Iab	-6.71
SMC 340	SMC	01:02:37.93	-72:35:54.66	no	C	4106	150	-0.95	0.17	G8	Iab	-6.49
SMC 342	SMC	01:02:40.74	-72:17:17.33	no	C	4055	142	-0.89	0.14	K0.5	Iab	-6.61
SMC 349	SMC	01:03:33.60	-72:03:02.26	no	C	4095	162	-0.66	0.15	K2	Ia-Iab	-7.51
SMC 351	SMC	01:03:37.31	-71:58:44.94	no	C	4199	276	-0.73	0.27	K0.5	Ia-Iab	-6.77
SMC 352	SMC	01:03:45.34	-72:07:49.09	no	C	4122	112	-0.75	0.11	K1	Iab	-6.73
SMC 354	SMC	01:03:53.85	-72:45:15.05	no	C	5108	158	-0.97	0.14	G1	Ib	-8.37
SMC 355	SMC	01:03:58.15	-72:49:56.77	no	C	4019	99	-0.84	0.09	K2	Iab-Ib	-6.52
SMC 358	SMC	01:04:06.85	-72:03:55.57	no	C	4047	259	-0.84	0.24	K1.5	Ia-Iab	-6.77
SMC 360	SMC	01:04:12.55	-71:59:13.80	no	C	4015	306	-0.71	0.24	K2	Iab	-6.65
SMC 367	SMC	01:04:32.18	-72:11:13.41	no	C	4115	154	-1.00	0.17	K0	Iab-Ib	-6.49
SMC 373	SMC	01:05:02.32	-72:55:32.57	no	C	4103	112	-0.81	0.12	K0	Iab	-6.68
SMC 375	SMC	01:05:27.40	-72:17:04.34	no	C	4117	258	-0.69	0.24	K0	Ia-Iab	-6.72
SMC 376	SMC	01:05:28.98	-72:40:21.55	no	C	4526	158	-0.93	0.22	G3	Iab	-6.86
SMC 381	SMC	01:07:02.21	-72:37:20.80	no	C	3689	112	-1.06	0.12	M1	Iab	-6.21
SMC 382	SMC	01:07:02.31	-72:35:34.31	no	C	4195	152	-0.90	0.17	G8	Iab	-6.35
SMC 390	SMC	01:07:39.55	-72:26:45.41	no	C	3949	65	-0.80	0.06	K5.5	Iab	-7.42
SMC 393	SMC	01:07:52.55	-72:10:42.07	no	C	4087	72	-0.63	0.07	K5	Ia-Iab	-7.80
SMC 398	SMC	01:09:17.90	-72:45:42.13	no	C	4193	146	-0.86	0.15	K2	Iab-Ib	-6.66
SXP4.78-A	SMC	00:52:30.53	-72:19:08.76	no	A	4514	449	-0.67	0.57	G6	Iab-Ib	-5.57
YSG002	SMC	00:35:03.25	-73:32:58.72	no	C	4652	365	-0.64	0.45	G6	Ib-II	-5.84
YSG003	SMC	00:41:16.06	-72:32:16.70	no	C	5077	189	-0.71	0.18	G6	Iab	-7.94
YSG004	SMC	00:41:43.45	-73:43:23.82	no	C	5590	245	-0.63	0.13	G0	Iab	-7.52
YSG006	SMC	00:46:02.39	-73:21:00.10	no	C	4907	454	-0.40	0.46	G5	Iab	-5.83
YSG007	SMC	00:46:49.82	-73:13:52.60	no	C	4448	390	-0.68	0.47	K0	Iab-Ib	-6.24
YSG008	SMC	00:46:53.06	-72:42:51.76	no	C	5100	428	-0.60	0.37	G0	Iab	-6.88
YSG010	SMC	00:47:08.66	-73:14:12.07	no	C	4454	319	-0.64	0.38	G6.5	Ia-Iab	-6.52

Table A2: continued.

ID	Cloud	RA J2000	DEC J2000	Var.	Epochs	T_{eff} (K)	ΔT_{eff} (K)	[M/H] (dex)	Δ [M/H] (dex)	SpT	LC	M_{bol} (mag)
YSG013	SMC	00:48:09.54	-72:21:28.56	no	C	4768	677	-0.53	0.73	G8	Iab	-5.90
YSG015	SMC	00:48:35.16	-72:22:10.42	no	C	4299	467	-0.84	0.59	G8	Iab	-6.40
YSG016	SMC	00:48:45.43	-72:55:27.40	no	C	4442	552	-0.77	0.71	G8	Iab	-5.89
YSG026	SMC	00:51:13.66	-72:33:01.68	no	C	4581	540	-0.62	0.70	G8	Ib	-5.86
YSG031	SMC	00:52:19.06	-73:09:23.10	no	C	5223	632	-0.22	0.47	G0	Iab	-5.93
YSG038	SMC	00:53:23.61	-72:47:01.32	no	C	4459	456	-0.71	0.63	G8	Iab	-6.45
YSG042	SMC	00:54:38.95	-72:21:19.83	no	C	4187	248	-0.75	0.26	G8	Ia-Iab	-6.65
YSG050	SMC	00:56:15.19	-71:52:31.15	no	C	4240	359	-0.71	0.37	K0	Iab	-6.12
YSG051	SMC	00:56:26.42	-73:28:23.32	no	C	4120	277	-0.80	0.25	K4	Ia-Iab	-6.86
YSG053	SMC	00:56:36.35	-72:26:46.42	no	C	4127	313	-0.84	0.29	G8.5	Ia-Iab	-6.57
YSG056	SMC	00:57:04.52	-72:29:40.28	no	C	4572	497	-0.67	0.63	G6.5	Ib	-5.85
YSG058	SMC	00:57:41.39	-72:37:52.25	no	C	4821	553	-0.28	0.56	G7	Ib	-5.87
YSG060	SMC	00:57:56.88	-73:33:43.57	no	C	4675	398	-0.68	0.52	G1	Ia-Iab	-6.95
YSG065	SMC	00:58:53.91	-72:12:04.82	no	C	4183	328	-0.86	0.33	G8	Ia-Iab	-6.54
YSG066	SMC	00:58:54.71	-72:50:59.69	no	C	4450	559	-0.57	0.65	G7	Iab	-5.89
YSG069	SMC	00:59:58.33	-72:34:18.89	no	C	4465	538	-0.70	0.68	G8	Iab	-6.00
YSG070	SMC	01:00:09.58	-72:33:59.36	no	C	4357	487	-0.75	0.58	K0	Ia-Iab	-6.28
YSG071	SMC	01:00:33.05	-72:11:28.95	no	C	4683	528	-0.27	0.57	K0	Ib	-5.93
YSG073	SMC	01:00:53.40	-72:29:02.18	no	C	4382	468	-0.73	0.57	G8	Iab	-6.38
YSG075	SMC	01:01:19.83	-72:17:04.28	no	C	4537	501	-0.53	0.61	G7.5	Ia-Iab	-5.99
YSG076	SMC	01:01:49.49	-72:05:45.38	no	C	4920	585	-0.61	0.63	G1	Iab	-6.12
YSG079	SMC	01:03:32.78	-72:24:56.67	no	C	4636	519	-0.56	0.66	G5.5	Iab	-6.05
YSG081	SMC	01:03:49.10	-73:42:44.46	no	C	4761	644	-0.49	0.67	G4.5	Iab	-5.97
YSG082	SMC	01:03:58.84	-72:23:09.06	no	C	4760	488	-0.83	0.64	G4	Iab	-6.19
YSG084	SMC	01:05:24.61	-72:55:29.30	no	C	4311	405	-0.64	0.44	G8	Iab	-6.42
YSG085	SMC	01:05:41.02	-72:21:24.55	no	C	4399	587	-0.66	0.71	G8	Ia-Iab	-6.01
YSG091	SMC	01:10:12.49	-72:37:31.02	no	C	4336	474	-0.46	0.47	G8.5	Ia-Iab	-6.38
LMC 002	LMC	05:21:03.95	-69:27:24.05	no	D	3665	132	-0.82	0.14	M3	Ib	-5.23
LMC 007	LMC	05:22:23.77	-69:22:52.11	no	D	3930	106	-0.39	0.06	K4.5	Iab-Ib	-6.34
LMC 008	LMC	05:22:43.66	-69:37:20.66	no	D	3877	122	-0.33	0.08	K5	Ib	-6.18
LMC 014	LMC	05:23:25.12	-69:25:35.53	no	D	3841	98	-0.44	0.07	K5	Ib	-6.23
LMC 020	LMC	05:23:47.94	-70:07:34.81	no	D	3715	116	-0.42	0.11	M2	Iab	-6.25
LMC 021	LMC	05:23:55.57	-68:54:36.34	no	D	3999	152	-0.75	0.14	K2	Ib	-5.26
LMC 022	LMC	05:23:56.27	-69:36:21.75	no	D	3756	97	-0.19	0.09	M2	Iab	-6.45
LMC 030	LMC	05:24:43.42	-70:00:01.18	no	D	3737	87	-0.35	0.08	M2.5	Iab	-6.73
LMC 033	LMC	05:24:56.81	-69:41:17.50	no	D	3825	87	-0.42	0.06	M0	Iab	-6.54
LMC 034	LMC	05:25:20.06	-69:20:24.18	no	D	4040	249	-0.75	0.21	K2	Ib-II	-4.56
LMC 035	LMC	05:25:24.89	-69:51:45.12	no	D	4530	204	-0.14	0.25	G5	Iab	-5.07
LMC 039	LMC	05:25:48.56	-68:56:23.51	no	D	3873	89	-0.35	0.06	M1	Ia	-6.65
LMC 042	LMC	05:25:55.76	-69:15:31.20	no	D	3993	131	-0.56	0.10	K3	Iab-Ib	-5.72
LMC 044	LMC	05:26:20.24	-69:30:12.36	no	D	3916	100	-0.42	0.06	K5	Iab-Ib	-6.43
LMC 045	LMC	05:26:23.54	-69:52:25.77	no	D	3682	73	-0.38	0.08	M3	Ia	-8.26
LMC 047	LMC	05:26:33.92	-69:22:30.49	no	D	3942	116	-0.18	0.06	K4	Iab	-6.30
LMC 048	LMC	05:26:43.92	-69:46:58.93	no	D	3853	181	-0.70	0.16	K3.5	Ib-II	-4.84
LMC 049	LMC	05:26:44.75	-69:06:06.53	no	D	4106	91	-0.16	0.06	K4	Iab	-7.08
LMC 050	LMC	05:26:53.18	-69:58:23.60	no	D	3726	241	-0.41	0.16	K5.5	Iab	-4.59
LMC 051	LMC	05:27:03.40	-69:05:19.56	no	D	4004	100	-0.36	0.06	K4	Iab-Ib	-6.34
LMC 055	LMC	05:27:15.36	-69:33:42.42	no	D	3844	149	-0.69	0.12	K4	Ib	-5.17
LMC 058	LMC	05:27:22.11	-69:47:10.22	no	D	3967	162	-0.52	0.12	K3	Ib	-5.34
LMC 060	LMC	05:27:38.60	-69:28:44.06	no	D	3705	92	-0.04	0.09	M1.5	Ia-Iab	-7.33
LMC 061	LMC	05:27:44.65	-69:47:51.47	no	D	3755	147	-0.17	0.11	M1.5	Iab	-5.97
LMC 063	LMC	05:27:51.72	-69:15:07.52	no	D	4113	113	-0.48	0.10	K0	Iab	-5.90
LMC 066	LMC	05:28:04.79	-69:03:56.78	no	D	4299	111	-0.33	0.12	G6	Iab	-6.07
LMC 070	LMC	05:28:20.92	-69:03:25.44	no	D	3701	104	-0.43	0.10	M2	Iab	-6.35
LMC 075	LMC	05:28:41.17	-70:07:15.58	no	D	3756	241	-0.44	0.16	K4.5	Iab	-4.86
LMC 076	LMC	05:28:41.18	-68:56:04.97	no	D	3759	117	-0.14	0.09	M2.5	Ib-II	-6.87
LMC 080	LMC	05:28:53.07	-69:30:15.02	no	D	4034	157	-0.65	0.14	K1	Ib	-5.14

Table A2: continued.

ID	Cloud	RA J2000	DEC J2000	Var.	Epochs	T_{eff} (K)	ΔT_{eff} (K)	[M/H] (dex)	Δ [M/H] (dex)	SpT	LC	M_{bol} (mag)
LMC 081	LMC	05:29:00.70	-69:26:44.06	no	D	3815	112	-0.43	0.09	K4.5	Ib	-6.15
LMC 082	LMC	05:29:01.23	-68:53:42.23	no	D	3891	91	-0.27	0.06	K4.5	Ib	-6.65
LMC 084	LMC	05:29:04.16	-69:21:18.75	no	D	4173	153	-0.29	0.12	K0	Iab	-5.58
LMC 088	LMC	05:29:29.04	-68:51:40.37	no	D	3923	91	-0.50	0.06	K4	Ib	-6.35
LMC 091	LMC	05:29:30.84	-68:47:58.72	no	D	3977	87	-0.61	0.07	K3	Ib	-6.25
LMC 092	LMC	05:29:34.32	-68:53:10.37	no	D	3846	117	-0.27	0.08	M2	Iab	-6.35
LMC 093	LMC	05:29:35.38	-68:30:45.51	no	D	3747	85	-0.21	0.08	M1.5	Iab	-6.94
LMC 094	LMC	05:29:40.31	-68:51:30.73	no	D	3879	95	-0.64	0.08	K5	Ib	-6.07
LMC 096	LMC	05:29:46.18	-68:37:02.45	no	D	3818	86	-0.54	0.07	M2	Ia-Iab	-6.76
LMC 101	LMC	05:30:01.75	-69:28:37.77	no	D	3810	104	-0.47	0.08	M0	Ib	-6.38
LMC 102	LMC	05:30:10.45	-70:04:10.90	no	D	3902	151	-0.22	0.09	K5	Iab	-5.98
LMC 111	LMC	05:30:38.49	-69:00:52.98	no	D	3851	103	-0.52	0.08	K4.5	Iab-Ib	-6.22
LMC 114	LMC	05:30:52.13	-69:25:42.59	no	D	3780	96	-0.40	0.08	M3	Ia-Iab	-6.45
LMC 116	LMC	05:30:56.67	-69:27:04.05	no	D	4022	106	-0.38	0.07	K4	Iab-Ib	-6.20
LMC 117	LMC	05:31:01.46	-69:59:28.63	no	D	3903	224	-0.50	0.16	K4.5	Ib	-5.03
LMC 120	LMC	05:31:18.36	-68:44:00.21	no	D	3992	85	-0.28	0.05	K4	Iab	-7.01
LMC 122	LMC	05:31:24.27	-68:41:33.65	no	D	3820	88	-0.45	0.06	K4.5	Ib-II	-6.85
LMC 124	LMC	05:31:30.82	-69:53:43.22	no	D	3935	125	-0.40	0.08	K4.5	Iab-Ib	-6.12
LMC 125	LMC	05:31:31.26	-69:10:28.50	no	D	4004	86	-0.31	0.05	K4	Iab-Ib	-6.69
LMC 127	LMC	05:31:33.40	-69:44:02.46	no	D	3651	181	-0.74	0.17	M2	Ib-II	-5.16
LMC 137	LMC	05:31:58.06	-69:13:53.42	no	D	3864	92	-0.40	0.06	K5.5	Ia-Iab	-6.71
LMC 140	LMC	05:32:02.13	-69:45:47.90	no	D	3815	131	-0.56	0.10	M0	Ia-Iab	-6.89
LMC 141	LMC	05:32:17.96	-69:15:03.74	no	D	3998	96	-0.49	0.07	K3	Iab-Ib	-6.52
LMC 143	LMC	05:32:20.55	-69:16:00.87	no	D	3825	78	-0.51	0.06	K5	Iab-Ib	-6.81
LMC 155	LMC	05:32:59.84	-69:18:21.63	no	D	3847	97	-0.39	0.06	K5	Iab-Ib	-6.56
LMC 156	LMC	05:33:00.19	-69:36:31.11	no	D	3858	99	-0.37	0.07	K5	Ib	-6.65
LMC 157	LMC	05:33:03.76	-69:19:41.11	no	D	3772	101	-0.41	0.09	M2	Iab	-6.49
LMC 159	LMC	05:33:11.46	-68:52:54.61	no	D	3907	105	-0.35	0.06	K4	Iab-Ib	-6.27
LMC 162	LMC	05:33:19.74	-69:21:39.65	no	D	3902	112	-0.57	0.08	K3.5	Iab-Ib	-6.00
LMC 164	LMC	05:33:25.78	-68:59:57.69	no	D	4075	97	-0.52	0.08	K2	Iab-Ib	-6.27
LMC 167	LMC	05:33:39.34	-69:10:52.64	no	D	3708	82	-0.12	0.08	M2.5	Iab	-6.45
LMC 168	LMC	05:33:41.15	-69:18:56.70	no	D	3733	92	-0.18	0.08	M2	Iab	-6.55
LMC 169	LMC	05:33:42.74	-70:06:57.56	no	D	3720	68	-0.62	0.07	M3	Ia-Iab	-7.10
LMC 175	LMC	05:34:01.55	-68:51:42.92	no	D	4000	92	-0.46	0.07	K4	Iab-Ib	-6.27
LMC 176	LMC	05:34:05.93	-70:07:05.17	no	D	3673	234	-0.56	0.20	M1	Ib-II	-4.58
LMC 179	LMC	05:34:18.36	-69:02:18.10	no	D	3971	104	-0.55	0.08	K3	Iab-Ib	-6.21
LMC 180	LMC	05:34:24.94	-69:23:36.66	no	D	3982	101	-0.16	0.04	K5	Ia-Iab	-7.25
LMC 182	LMC	05:34:28.19	-70:17:13.24	no	D	4014	174	-0.45	0.13	K4	Ib	-5.39
LMC 183	LMC	05:34:29.37	-69:07:54.72	no	D	3787	99	-0.38	0.08	K5	Iab-Ib	-6.43
LMC 187	LMC	05:34:42.97	-69:12:27.23	no	D	3896	102	-0.37	0.06	K4.5	Iab	-6.39
LMC 189	LMC	05:34:49.97	-69:19:51.00	no	D	4047	103	-0.51	0.09	K2	Iab-Ib	-5.98
LMC 194	LMC	05:34:53.77	-69:08:02.08	no	D	4509	108	-0.01	0.13	G3	Ia	-6.18
LMC 195	LMC	05:34:59.80	-69:12:36.87	no	D	3903	103	-0.47	0.08	K4	Iab-Ib	-6.33
LMC 198	LMC	05:35:21.76	-69:13:39.75	no	D	3972	85	-0.55	0.06	K4	Iab	-6.60
LMC 199	LMC	05:35:21.78	-69:42:46.71	no	D	3720	96	-0.06	0.09	M1.5	Ia-Iab	-7.15
LMC 200	LMC	05:35:22.25	-69:02:23.07	no	D	3904	92	-0.33	0.05	M0	Iab	-6.70
LMC 201	LMC	05:35:23.52	-69:56:50.95	no	D	3667	164	-0.70	0.15	M2	Ib-II	-5.01
LMC 202	LMC	05:35:26.31	-69:28:02.20	no	D	3783	79	-0.56	0.07	M3	Iab	-7.06
LMC 203	LMC	05:35:29.30	-69:43:53.37	no	D	3864	97	-0.37	0.06	K5	Ib	-6.54
LMC 207	LMC	05:35:41.10	-69:11:59.63	no	D	3882	87	-0.39	0.05	M0	Ia-Iab	-7.14
LMC 209	LMC	05:35:49.42	-69:04:55.45	no	D	3981	100	-0.42	0.07	K4	Iab	-6.40
LMC 211	LMC	05:35:50.30	-69:37:08.00	no	D	3821	121	-0.27	0.09	M2	Iab	-7.21
LMC 213	LMC	05:35:56.28	-69:17:50.78	no	D	3907	205	-0.02	0.08	M2.5	Ia-Iab	-6.81
LMC 215	LMC	05:36:04.57	-69:29:26.91	no	D	3977	119	-0.33	0.07	K4	Iab-Ib	-6.07
LMC 216	LMC	05:36:07.92	-69:12:33.06	no	D	3909	96	-0.33	0.06	K4	Iab-Ib	-6.60
LMC 218	LMC	05:36:26.03	-69:19:29.14	no	D	3876	102	-0.33	0.07	M0.5	Iab	-6.76
LMC 220	LMC	05:36:31.13	-69:50:07.53	no	D	3749	113	-0.31	0.10	M2	Ib-II	-6.28

Table A2: continued.

ID	Cloud	RA J2000	DEC J2000	Var.	Epochs	T_{eff} (K)	ΔT_{eff} (K)	[M/H] (dex)	Δ [M/H] (dex)	SpT	LC	M_{bol} (mag)
LMC 224	LMC	05:36:47.52	-69:10:10.37	no	D	3911	109	-0.37	0.07	K4	Iab-Ib	-6.25
LMC 225	LMC	05:36:48.18	-69:16:42.39	no	D	3848	105	-0.50	0.08	K5	Iab-Ib	-6.22
LMC 226	LMC	05:36:48.48	-69:14:35.42	no	D	3912	113	-0.32	0.07	K4.5	Ia-Iab	-6.72
LMC 228	LMC	05:36:55.63	-68:53:26.22	no	D	3939	110	-0.76	0.10	K4	Ib	-6.04
LMC 230	LMC	05:37:13.51	-69:08:34.60	no	D	3748	79	-0.54	0.08	M3	Ia-Iab	-6.96
LMC 231	LMC	05:37:35.98	-69:12:29.82	no	D	3894	91	-0.61	0.07	K4	Iab-Ib	-6.37
LMC 232	LMC	05:37:47.46	-68:36:20.60	no	D	3890	96	-0.45	0.06	K4	Iab-Ib	-6.64
LMC 234	LMC	05:37:54.64	-69:09:03.27	no	D	3867	106	-0.38	0.07	K4.5	Iab-Ib	-6.35
LMC 236	LMC	05:38:06.56	-69:28:45.24	no	D	3846	121	-0.15	0.07	K5	Iab	-6.57
LMC 237	LMC	05:38:06.59	-69:03:45.22	no	D	3950	105	-0.67	0.08	K4	Iab-Ib	-6.12
LMC 239	LMC	05:38:17.01	-69:04:00.98	no	D	4005	80	-0.57	0.06	K4	Iab	-6.57
LMC 242	LMC	05:38:25.99	-69:22:43.49	no	D	3863	88	-0.41	0.06	K5	Iab-Ib	-6.64
LMC 243	LMC	05:38:26.71	-69:08:52.73	no	D	3737	94	-0.15	0.09	K5	Ia-Iab	-6.90
LMC 244	LMC	05:38:34.53	-69:34:39.63	no	D	3873	114	-0.28	0.07	M1	Ia-Iab	-6.88
LMC 250	LMC	05:39:04.25	-69:36:03.92	no	D	3767	112	-0.22	0.09	M0.5	Iab	-7.19
LMC 252	LMC	05:39:32.34	-69:34:50.10	no	D	3695	66	0.27	0.07	M0	Ia-Iab	-8.21
LMC 256	LMC	05:40:49.87	-69:22:45.52	no	D	3848	117	-0.47	0.09	M1	Iab	-7.15
LMC 257	LMC	05:40:53.37	-69:45:24.88	no	D	3778	232	-0.52	0.19	M1.5	Iab	-6.38
LMC 258	LMC	05:40:55.86	-69:41:36.37	no	D	3888	198	-0.28	0.12	K5.5	Iab	-6.31
LMC 260	LMC	05:41:08.17	-69:55:45.94	no	D	3979	233	-0.37	0.15	K4.5	Iab-Ib	-6.52
LMC 261	LMC	05:41:13.71	-69:34:03.10	no	D	3998	168	-0.21	0.09	K4	Iab-Ib	-6.38
LMC 262	LMC	05:41:33.37	-69:47:40.51	no	D	3744	125	-0.15	0.11	M2	Iab	-7.33
LMC 263	LMC	05:42:07.08	-69:02:53.25	no	D	4021	216	-0.71	0.19	K2.5	Iab	-6.15
124836	LMC	05:21:43.88	-69:21:25.54	no	D	3859	113	-0.41	0.08	K5	Iab	-6.29
128130	LMC	05:22:31.10	-69:34:05.16	no	A, D	3801	86	-0.39	0.06	M2	Ia-Iab	-6.87
130426	LMC	05:23:02.77	-69:20:37.03	no	A, D	3758	75	-0.26	0.07	M2	Iab	-7.03
131735	LMC	05:23:34.00	-69:19:06.81	yes	A	4084	340	-0.32	0.22	K2	Iab-Ib	-6.88
131735	LMC	05:23:34.00	-69:19:06.81	yes	D	4087	90	-0.33	0.06	K3.5	Ia-Iab	-6.88
135754	LMC	05:26:28.22	-69:07:57.60	yes	A	3778	238	-0.29	0.17	M2.5	Iab	-7.05
135754	LMC	05:26:28.22	-69:07:57.60	yes	D	3767	97	-0.13	0.08	M1	Iab	-7.05
136348	LMC	05:26:42.08	-68:56:38.73	no	A	3721	183	-0.56	0.15	M0	Iab-Ib	-6.96
136378	LMC	05:26:42.72	-68:57:13.17	no	A, D	3860	82	-0.36	0.05	M2	Ia-Iab	-7.06
137624	LMC	05:27:10.31	-69:16:17.56	yes	A	3851	204	-0.32	0.14	M2	Iab	-6.87
137624	LMC	05:27:10.31	-69:16:17.56	yes	D	3911	78	-0.40	0.05	K5	Iab	-6.87
137818	LMC	05:27:14.23	-69:11:10.74	yes	D	3903	73	-0.50	0.05	M2	Ia	-7.30
138405	LMC	05:27:26.74	-69:00:01.89	no	A, D	3828	80	-0.35	0.06	K5	Iab-Ib	-6.94
138475	LMC	05:27:28.05	-69:00:36.09	no	A	3858	225	-0.35	0.15	K5	Iab-Ib	-7.26
139027	LMC	05:27:39.65	-69:09:01.21	yes	A	3813	209	-0.23	0.14	M2	Iab	-7.61
139027	LMC	05:27:39.65	-69:09:01.21	yes	D	3857	103	-0.24	0.06	M0.5	Iab	-7.61
139591	LMC	05:27:51.13	-69:10:46.02	yes	A	3723	156	-0.43	0.13	M3	Ia	-7.21
139591	LMC	05:27:51.13	-69:10:46.02	yes	D	3803	89	-0.24	0.07	M1.5	Ib-II	-7.21
140006	LMC	05:28:00.05	-69:07:42.41	yes	D	4108	71	-0.12	0.04	M2	Ia	-6.70
140403	LMC	05:28:08.06	-69:13:10.99	yes	D	3786	72	-0.75	0.07	M3	Ia	-7.47
140782	LMC	05:28:15.89	-69:12:00.98	no	A, D	3775	73	-0.36	0.05	M2	Iab	-7.03
140912	LMC	05:28:18.59	-69:07:34.81	yes	A	3842	193	-0.38	0.13	M0	Iab	-7.17
140912	LMC	05:28:18.59	-69:07:34.81	yes	D	3711	78	-0.44	0.08	M3	Ia-Iab	-7.17
141377	LMC	05:28:27.93	-69:12:57.34	no	D	5002	122	0.26	0.12	G2	Ia	-7.98
SP77 46–32	LMC	05:28:28.86	-68:07:07.89	no	A	3947	173	-0.42	0.12	M2	Ia	-8.05
141507	LMC	05:28:30.34	-69:00:44.47	yes	A	3913	219	-0.52	0.17	K4	Iab-Ib	-7.00
141507	LMC	05:28:30.34	-69:00:44.47	yes	D	3862	88	-0.32	0.06	M0	Iab	-7.00
SP77 46–31	LMC	05:28:36.60	-68:42:38.49	no	A, D	3738	74	-0.14	0.07	M2.5	Ia-Iab	-7.59
142202	LMC	05:28:45.48	-68:58:02.28	yes	A	3892	166	-0.11	0.09	K3	Iab	-7.94
142202	LMC	05:28:45.48	-68:58:02.28	yes	D	3751	91	-0.38	0.08	M3	Iab	-7.94
142907	LMC	05:29:00.78	-68:46:33.52	no	A, D	3731	70	-0.48	0.07	M3	Iab	-7.10
143035	LMC	05:29:03.48	-69:06:46.19	no	A, D	3954	119	-0.94	0.13	M3.5	Ia	-7.56
143280	LMC	05:29:08.40	-69:12:18.39	no	A, D	3768	76	-0.15	0.06	M2	Iab	-7.20

Table A2: continued.

ID	Cloud	RA J2000	DEC J2000	Var.	Epochs	T_{eff} (K)	ΔT_{eff} (K)	[M/H] (dex)	$\Delta[M/H]$ (dex)	SpT	LC	M_{bol} (mag)
143877	LMC	05:29:21.00	-68:47:31.37	no	A, D	3972	104	-0.09	0.05	K4.5	Iab	-7.74
143898	LMC	05:29:21.43	-69:00:20.21	yes	A	4001	146	-0.34	0.11	K4	Ia-Iab	-7.83
143898	LMC	05:29:21.43	-69:00:20.21	yes	D	3904	138	-0.10	0.06	K5.5	Iab	-7.83
SP77 46-40	LMC	05:29:21.54	-68:44:11.17	no	A, D	3851	82	-0.31	0.05	K4.5	Iab-Ib	-7.08
144217	LMC	05:29:27.58	-69:08:50.28	no	A, D	3843	76	-0.59	0.06	M3	Ia	-8.25
145013	LMC	05:29:42.21	-68:57:17.37	no	A, D	3664	75	0.06	0.07	M2.5	Ia-Iab	-8.75
145112	LMC	05:29:43.96	-69:05:49.89	yes	A	3957	139	-0.25	0.09	M1.5	Ia	-7.67
145112	LMC	05:29:43.96	-69:05:49.89	yes	D	3842	82	-0.62	0.06	M3	Ia-Iab	-7.67
145716	LMC	05:29:54.75	-69:04:15.68	no	A, D	4041	82	-0.19	0.04	K5	Iab	-7.26
146244	LMC	05:30:04.59	-68:47:28.86	no	A, D	3975	79	-0.30	0.05	K4	Iab-Ib	-6.87
146266	LMC	05:30:04.94	-69:03:59.72	no	A, D	3840	89	-0.26	0.06	M0	Iab-Ib	-6.76
146548	LMC	05:30:09.57	-69:11:03.66	yes	A	3789	164	-0.52	0.13	K4	Iab-Ib	-6.81
146548	LMC	05:30:09.57	-69:11:03.66	yes	D	3806	99	-0.25	0.07	K5.5	Iab-Ib	-6.81
147479	LMC	05:30:26.29	-69:30:24.34	no	A, D	3715	60	0.05	0.06	M1	Ia-Iab	-7.06
148409	LMC	05:30:41.99	-69:05:23.19	no	A, D	3775	68	-0.38	0.07	M2.5	Iab	-6.77
149560	LMC	05:31:00.46	-69:10:40.01	no	A, D	3985	119	-0.60	0.09	K4	Iab-Ib	-5.92
149721	LMC	05:31:03.44	-69:05:40.06	no	A, D	3971	90	-0.23	0.04	K5	Iab-Ib	-7.05
149767	LMC	05:31:04.18	-69:19:03.07	no	A, D	3792	153	-0.43	0.11	M3.5	Ia	-7.65
150396	LMC	05:31:15.45	-69:03:58.87	no	A, D	3720	67	-0.22	0.07	M2.5	Ia-Iab	-7.26
150577	LMC	05:31:18.43	-69:09:28.21	no	A, D	3916	99	-0.30	0.06	K5	Iab	-6.88
150976	LMC	05:31:25.61	-69:21:17.90	no	A, D	3750	68	-0.23	0.06	M1.5	Iab	-6.85
154311	LMC	05:32:27.42	-69:16:52.61	yes	A	3848	145	-0.31	0.10	M2	Ia-Iab	-7.58
154311	LMC	05:32:27.42	-69:16:52.61	yes	D	3811	95	-0.16	0.07	M0.5	Iab	-7.58
154542	LMC	05:32:31.33	-69:20:25.47	no	A, D	3761	76	-0.33	0.07	M1	Iab-Ib	-6.92
154729	LMC	05:32:35.30	-69:07:51.67	no	A, D	3732	72	-0.33	0.07	M2.5	Ia-Iab	-7.18
SP77 53-3	LMC	05:32:59.85	-68:35:54.86	no	A, D	4018	85	-0.12	0.04	K5	Ia-Iab	-7.98
158646	LMC	05:33:52.17	-69:11:13.52	yes	A	4011	186	-0.23	0.11	K5	Ia	-7.44
158646	LMC	05:33:52.17	-69:11:13.52	yes	D	3713	76	-0.26	0.09	M3	Ia	-7.44
159893	LMC	05:34:19.48	-68:59:36.77	no	A, D	3822	79	-0.39	0.06	M1.5	Iab	-7.03
159974	LMC	05:34:21.43	-69:22:00.25	yes	A	3969	255	-0.78	0.21	K2	Iab	-6.77
159974	LMC	05:34:21.43	-69:22:00.25	yes	D	3941	92	-0.58	0.06	K4.5	Iab	-6.77
160518	LMC	05:34:33.78	-69:15:02.36	no	A, D	3767	70	-0.44	0.06	M2	Iab	-7.19
161078	LMC	05:34:47.02	-69:29:00.59	no	A, D	3855	92	-0.38	0.06	K5	Iab-Ib	-6.61
162635	LMC	05:35:24.52	-69:04:03.43	yes	A	3986	158	-0.45	0.13	M1	Iab	-7.09
162635	LMC	05:35:24.52	-69:04:03.43	yes	D	3804	69	-0.62	0.06	M3	Ia-Iab	-7.09
163007	LMC	05:35:32.81	-69:04:19.20	no	A, D	3851	79	-0.34	0.06	M0	Iab	-7.20
163466	LMC	05:35:43.80	-68:51:20.95	no	A, D	3872	86	-0.21	0.05	M1	Ia-Iab	-7.55
163814	LMC	05:35:51.96	-69:22:29.04	yes	A	3843	198	-0.60	0.17	K3	Ia-Iab	-7.09
163814	LMC	05:35:51.96	-69:22:29.04	yes	D	3845	84	-0.48	0.06	K5	Iab-Ib	-7.09
164506	LMC	05:36:06.35	-68:56:40.76	yes	A	3886	139	-0.49	0.10	K5	Ia-Iab	-7.11
164506	LMC	05:36:06.35	-68:56:40.76	yes	D	3794	85	-0.33	0.07	M1	Ib-II	-7.11
164709	LMC	05:36:10.61	-68:54:40.16	no	A, D	3757	159	-0.57	0.13	M3.5	Ia-Iab	-7.49
165242	LMC	05:36:20.38	-68:56:18.63	no	A, D	3751	67	-0.77	0.07	M3	Ia-Iab	-6.96
165543	LMC	05:36:26.79	-69:23:51.41	no	D	4734	132	-0.23	0.16	G1	Ia	-8.40
166155	LMC	05:36:40.60	-69:23:16.39	no	A, D	3966	79	-0.51	0.05	K4	Iab	-6.80
168047	LMC	05:37:20.50	-69:19:38.64	no	A, D	3953	64	-0.49	0.04	K4	Iab	-7.24
168290	LMC	05:37:26.36	-68:47:40.29	yes	A	3794	174	-0.42	0.13	M2	Ia-Iab	-7.25
168290	LMC	05:37:26.36	-68:47:40.29	yes	D	3836	96	-0.27	0.07	M0	Ia-Iab	-7.25
168469	LMC	05:37:30.65	-69:02:33.18	no	A, D	4012	71	-0.51	0.06	K3.5	Iab	-6.72
168757	LMC	05:37:36.82	-69:29:23.44	yes	A	3801	133	-0.67	0.11	M0.5	Ib	-7.19
169049	LMC	05:37:43.04	-69:24:59.96	yes	D	3688	72	-0.09	0.08	M2	Ia-Iab	-7.59
169754	LMC	05:37:58.67	-69:14:23.99	no	A, D	4572	75	0.19	0.09	G5	Ia	-7.12
170079	LMC	05:38:06.65	-69:17:29.69	yes	A	3648	150	-0.38	0.14	M1	Ia-Iab	-7.34
170539	LMC	05:38:18.12	-69:17:42.60	no	D	3668	83	-0.28	0.09	M3	Ia-Iab	-7.05
173854	LMC	05:39:46.13	-69:19:28.23	no	D	3690	96	-0.45	0.10	M3	Ia-Iab	-6.95
174324	LMC	05:40:07.62	-69:20:04.95	no	D	3745	129	-0.55	0.12	M3	Iab	-7.17

Table A2: continued.

ID	Cloud	RA J2000	DEC J2000	Var.	Epochs	T_{eff} (K)	ΔT_{eff} (K)	[M/H] (dex)	$\Delta[M/H]$ (dex)	SpT	LC	M_{bol} (mag)
174543	LMC	05:40:16.98	-69:27:53.85	no	D	3824	102	-0.54	0.08	M3	Ia	-7.28
174714	LMC	05:40:24.45	-69:21:17.00	no	A, D	3752	82	-0.19	0.07	M2	Ia-Iab	-7.51
174742	LMC	05:40:25.32	-69:15:30.21	no	A, D	4013	146	-0.01	0.06	M0	Ia-Iab	-6.92
175015	LMC	05:40:36.93	-69:26:20.33	yes	A	3757	176	-0.32	0.14	M2.5	Ia-Iab	-7.16
175188	LMC	05:40:43.76	-69:21:58.17	no	A, D	3677	84	-0.76	0.08	M3	Ib	-7.85
175464	LMC	05:40:55.33	-69:23:25.23	no	D	3718	120	-0.50	0.12	M3	Iab	-7.83
SP77 54-35	LMC	05:40:59.19	-69:26:10.91	no	A	3781	168	-0.49	0.14	M0.5	Iab-Ib	-7.09
175709	LMC	05:41:05.06	-69:04:42.38	no	A, D	3874	97	-0.35	0.06	K5	Iab	-7.42
175746	LMC	05:41:06.89	-69:17:14.72	no	D	3704	67	0.07	0.07	M2	Iab	-7.70
SP77 54-38	LMC	05:41:10.66	-69:38:04.06	yes	A	3843	245	-0.35	0.17	M1	Iab	-7.86
176135	LMC	05:41:21.68	-69:31:48.90	no	D	3901	105	-0.62	0.08	M2.5	Ia	-7.66
176216	LMC	05:41:24.55	-69:18:12.89	no	D	3862	113	-0.41	0.08	K5	Iab-Ib	-6.45
176335	LMC	05:41:29.56	-69:27:16.11	no	A, D	3986	121	-0.34	0.08	K4	Ib	-7.07
176695	LMC	05:41:43.31	-69:28:15.41	no	D	3850	145	-0.22	0.10	M0	Iab	-7.14
176715	LMC	05:41:44.02	-69:12:02.76	no	D	3939	153	-0.47	0.12	K5	Ia-Iab	-7.07
176890	LMC	05:41:50.10	-69:21:15.60	no	D	3928	186	-0.26	0.11	K5	Ia-Iab	-7.08
177150	LMC	05:42:00.72	-69:11:36.97	no	D	3792	141	-0.37	0.11	M2	Iab	-6.75
178066	LMC	05:42:38.56	-69:09:51.42	no	D	3956	133	-0.32	0.08	K5.5	Ia-Iab	-6.73

This paper has been typeset from a $\text{T}_{\text{E}}\text{X}/\text{L}^{\text{A}}\text{T}_{\text{E}}\text{X}$ file prepared by the author.